arXiv:astro-ph/0003087v1 7 Mar 2000

Kinematics of Metal-Poor Stars in the Galaxy. III. Formation of the Stellar Halo and Thick Disk as Revealed from a Large Sample of Non-Kinematically Selected Stars

Masashi Chiba
National Astronomical Observatory, Mitaka, Tokyo 181-8588, Japan
email: chibams@gala.mtk.nao.ac.jp

Timothy C. Beers
Department of Physics & Astronomy, Michigan State University, E. Lansing, MI 48824
email: beers@pa.msu.edu

ABSTRACT

We present a detailed analysis of the space motions of 1203 solar-neighborhood stars with metal abundances [Fe/H] ≤ -0.6, on the basis of a recently revised and supplemented catalog of metal-poor stars selected without kinematic bias (Beers et al. 2000). This sample, having available proper motions, radial velocities, and distance estimates for stars with a wide range of metal abundances, is by far the largest such catalog to be assembled to date.

We show that the stars in our sample with [Fe/H] ≤ -2.2, which likely represent a "pure" halo component, are characterized by a radially elongated velocity ellipsoid $(\sigma_U, \sigma_V, \sigma_W) = (141 \pm 11, 106 \pm 9, 94 \pm 8)$ km s^{-1} and small prograde rotation $< V_\phi >= 30$ to 50 km s^{-1}, consistent with previous analysis of this sample based on radial velocity information alone (Beers & Sommer-Larsen 1995). In contrast to the previous analysis, we find a decrease in $< V_\phi >$ with increasing distance from the Galactic plane for stars which are likely to be members of the halo population ($\Delta < V_\phi > /\Delta|Z| = -52 \pm 6$ km s^{-1} kpc^{-1}), which may represent the signature of a dissipatively formed flattened inner halo.

Unlike essentially all previous kinematically selected catalogs, the metal-poor stars in our sample exhibit a diverse distribution of orbital eccentricities, e, with no apparent correlation between [Fe/H] and e. This demonstrates, clearly and convincingly, that the evidence offered by Eggen, Lynden-Bell, and Sandage (1962) for a rapid collapse of the Galaxy, an apparent correlation between the orbital eccentricity of halo stars with metallicity, is basically the result of their proper-motion selection bias. However, even in our non-kinematically selected sample, we have identified a small concentration of high-e stars at [Fe/H] ~ -1.7, which may originate, in part, from infalling gas during the early formation of the Galaxy.

We find no evidence for an additional thick disk component for stellar abundances [Fe/H] ≤ -2.2. The kinematics of the intermediate-abundance stars close to the Galactic plane are, in part, affected by the presence of a rapidly rotating thick

disk component with $< V_\phi > \simeq 200$ km s^{-1} (with a vertical velocity gradient on the order of $\Delta < V_\phi > /\Delta|Z| = -30 \pm 3$ km s^{-1} kpc^{-1}), and velocity ellipsoid $(\sigma_U, \sigma_V, \sigma_W) = (46 \pm 4, 50 \pm 4, 35 \pm 3)$ km s^{-1}. The fraction of low-metallicity stars in the solar neighborhood which are members of the thick disk population is estimated as $\sim 10\%$ for $-2.2 <$ [Fe/H] ≤ -1.7 and $\sim 30\%$ for $-1.7 <$ [Fe/H] ≤ -1. We obtain an estimate of the radial scale length of the metal-weak thick disk of 4.5 ± 0.6 kpc.

We also analyze the global kinematics of the stars constituting the halo component of the Galaxy. The outer part of the halo, which we take to be represented by local stars on orbits reaching more than 5 kpc from the Galactic plane, exhibits no systematic rotation. In particular, we show that previous suggestions of the presence of a "counter-rotating high halo" are *not* supported by our analysis. The density distribution of the outer halo is nearly spherical, and exhibits a power-law profile that is accurately described as $\rho \propto R^{-3.55 \pm 0.13}$. The inner part of the halo is characterized by a prograde rotation and a highly flattened density distribution. We find no distinct boundary between the inner and outer halo.

We confirm the clumping in angular-momentum phase space of a small number of local metal-poor stars noted by Helmi et al. (1999). We also identify an additional elongated feature in angular-momentum phase space extending from the clump to regions with high azimuthal rotation. The number of members in the detected clump is not significantly increased from that reported by Helmi et al., even though the total number of the sample stars we consider is almost triple that of the previous investigation. We conclude that the fraction of halo stars that may have arisen from the precursor object of this clump may be smaller than 10% of the present Galactic halo, as previously suggested.

The implications of our results for the formation of the Galaxy are discussed, in particular in the context of the currently favored Cold Dark Matter theory of hierarchical galaxy formation.

Subject headings: Galaxy: evolution – Galaxy: halo — Galaxy: abundances — Stars: Population II

1. Introduction

Over the past few decades, studies of the luminous halo population of metal-deficient field stars and globular clusters have provided an increasingly detailed picture of the formation and evolution of the Galaxy. Because the time required for mixing of the initial phase-space distribution of these objects, via exchange of energies and angular momenta, is thought to exceed the age of the Galaxy, kinematic information obtained at the present enables one to elucidate the initial dynamical conditions under which these objects were born. To the extent one is able to

estimate ages of these halo population objects, either directly (which is difficult at present), or indirectly (by postulating that the *ensemble* metallicities of these objects increases with time), their formation history is obtainable as well. Thus, the dynamical and chemical state of these halo-population objects provides important information on how the Galaxy has developed its characteristic structures during the course of its evolution.

Almost forty years ago, the "canonical" scenario of the early dynamical evolution of the Galaxy was put forward by Eggen, Lynden-Bell, & Sandage (1962, hereafter ELS) to explain what they believed to be an observed correlation between the orbital characteristics and metal abundances of stars in the solar neighborhood. Focusing on the lack of metal-poor stars with low eccentricity orbits in their (proper-motion selected) sample, ELS argued that the Galaxy must have undergone a rapid collapse, then formed a rotationally supported disk. Although criticism of the ELS model has been levied because of the potential influence of their kinematic selection bias, especially the extent to which this might alter the derived collapse timescale of the early Galaxy (Yoshii & Saio 1979; Norris, Bessell, & Pickles 1985; Norris 1986; Norris & Ryan 1991; Beers & Sommer-Larsen 1995, hereafter BSL; Chiba & Yoshii 1998, hereafter CY), the ELS collapse picture has long been influential for studies of disk galaxies like our own, and for elliptical galaxies as well (e.g., Larson 1974; van Albada 1982).

An alternative picture for the formation of the Galactic halo was proposed by Searle & Zinn (1978, hereafter SZ), who noted a number of difficulties in reconciling several observed properties of the halo globular cluster system with predictions of the ELS model. Among these, the existence of a large (several Gyr) spread in the inferred ages of the Galactic globulars, and the lack of an abundance gradient with distance from the Galactic center were thought to be the most crucial. SZ suggested that, in its earliest epochs, the halo component of the Galaxy may have experienced prolonged, chaotic accretion of subgalactic fragments. More recent studies of halo field stars also provide evidence which may support the SZ picture, including a possible age spread among halo subdwarfs (e.g., Schuster & Nissen 1989; Carney et al. 1996), a gradient in the inferred ages of field horizontal-branch (FHB) stars and RR Lyrae variables, in the sense that the outer halo FHB stars and RR Lyrae variables appear several Gyr younger than those of the inner halo (Preston, Shectman, & Beers 1991; Lee & Carney 1999), a report of the apparent clustering of FHB stars in the halo (Doinidis & Beers 1989), possible kinematic substructure in the halo (e.g., Doinidis & Beers 1989; Majewski, Munn, & Hawley 1994; 1996), and distinct changes in the kinematics of the field populations as one moves from the inner to outer halo (e.g., Majewski 1992; Carney et al. 1996; Sommer-Larsen et al. 1997).

In order to assess which picture, ELS or SZ (or both, e.g., Norris 1994; Freeman 1996; Carney et al. 1996), more correctly describes the early history of the Galaxy, we require a large and reliable set of data for halo-population objects chosen with criteria that do not unduly influence the subsequent analysis. As we show, the analysis of stars chosen with a kinematic selection bias can be particularly troublesome. Interestingly, in order to obtain adequately large samples of stars exhibiting a range of metallicities in the solar neighborhood, an abundance bias is actually

required, otherwise the exceedingly rare very low-metallicity stars of the halo population will not be represented in sufficient numbers. One must exercise caution, however, that abundance estimates for stars in the sample under consideration are as accurate as possible, due to the presence of an overlap of the local halo with the relatively high density thick-disk population (e.g., Anthony-Twarog & Twarog 1994; BSL; Ryan & Lambert 1995; Twarog & Anthony-Twarog 1996; CY). It is similarly important to assemble a large and homogeneously analyzed sample, both to minimize statistical fluctuations in the derived kinematic quantities, and to reduce the effects of other systematic errors (such as might arise in estimates of stellar distances).

In this paper we present an analysis of the kinematics of metal-deficient field stars in the solar neighborhood, based on a large catalog of stars selected without kinematic bias (Beers et al. 2000, hereafter Paper II). This catalog, consisting of 2041 stars from the published literature with abundances [Fe/H]≤ -0.6, includes updated stellar positions, newly derived homogeneous distance estimates, revised radial velocities, and refined metal abundance estimates. Moreover, a subset of some 1200 stars in the catalog now have available proper motions, taken from a variety of recently completed proper motion catalogs. We note that this catalog is (by far) the largest sample of metal-deficient field stars with available proper motions among any previously assembled non-kinematically selected samples. Thus, it is now possible to draw a much more definitive picture of the early kinematic evolution of the Galaxy.

Our paper is organized as follows. In §2 we present a discussion of the detailed velocity distributions of our sample stars, concentrating on those presently located in the solar neighborhood. In §3 we analyze the orbital motions of these stars. In §4 we consider the global character of the halo of the Galaxy, as deduced from the kinematics of a local sample. In §5, we further examine evidence for kinematic substructure in the phase-space distribution of the halo. Finally, in §6, the results of the present work are summarized, and their implications for the formation and evolution of the Galaxy are discussed.

2. Velocity Distributions of the Metal-Poor Stars

2.1. Individual and Mean Space Velocities

Paper II of this series presented proper motions for 1214 stars with [Fe/H] ≤ -0.6, as well as for a number of slightly more metal-rich stars. Within this sample, 1203 stars with [Fe/H] ≤ -0.6 have distance estimates and radial velocities as well as proper motions, so that the full three-dimensional velocities are directly calculable. Figure 1 is a reproduction of Figure 8 from Paper II, and shows the local velocity components vs. [Fe/H] for these 1203 stars. The velocity components U, V, and W are directed to the Galactic anticenter, rotation direction, and north Galactic pole, respectively, and have been corrected for the local solar motion $(U_\odot, V_\odot, W_\odot) = (-9, 12, 7)$ km s^{-1} with respect to the local standard of rest (LSR) (Mihalas & Binney 1981). Note the excellent coverage of this sample over the entire range of Galactic

abundances, especially below [Fe/H] = −2 and above [Fe/H] = −1, where previous studies that made use of, for example, the sample of metal-poor stars studied with *Hipparcos*, lack sufficient numbers of stars (compare, e.g., with Figure 4 of CY).

To examine the characteristic *local* velocity distributions of our sample, we confine ourselves to a discussion of the stars for which the Galactocentric distance along the plane, R, is between 7 and 10 kpc, and those for which the distance from the Sun, D, is within 4 kpc. Six stars in this subsample have large rest-frame velocities, $V_{RF} > 550$ km s^{-1}, that are in excess of the canonical escape velocity in the solar neighborhood ($V_{esc} \sim 500 - 550$ km s^{-1}; Carney, Latham, & Laird 1988). Although some of the space velocities may indeed be this high, the majority of these stars probably have large V_{RF} due to an over-estimation of their distances, which has artificially inflated their estimated tangential velocities. We choose to remove these extreme-velocity stars by placing an additional limit of $V_{RF} \leq 550$ km s^{-1} on the sample. The stars satisfying the above selection criteria are referred to as the "Selected Sample" in the following discussion.

We first calculate the mean velocities ($< U >, < V >, < W >$) and velocity dispersions ($\sigma_U, \sigma_V, \sigma_W$) for the Selected Sample – values for five characteristic ranges in metal abundance are listed in Table 1a. Velocity dispersions are estimated from the standard deviations, after correction for the typical measurement errors in the velocities (~ 10 km s^{-1}). Figure 2 shows ($\sigma_U, \sigma_V, \sigma_W$) as a function of [Fe/H]. In this Figure we have adopted a finer binning in metal abundance; the dispersion measurements in each bin are listed in Table 1b. The filled and open circles in Figure 2 denote the stars at $|Z| < 1$ kpc and $|Z| < 4$ kpc, respectively, where Z is the height above the Galactic plane.

The most metal-deficient stars in the Selected Sample, those more metal-poor than [Fe/H] = −2.2, are dominated by members of the halo population. For $|Z| < 1$ kpc, these stars exhibit a radially elongated velocity ellipsoid $(\sigma_U, \sigma_V, \sigma_W) = (141 \pm 11, 106 \pm 9, 94 \pm 8)$ km s^{-1}, in good agreement with previous results (e.g., BSL; CY). With a slightly more metal-rich cut on the abundances, i.e., selecting stars with [Fe/H] < −1.7, we obtain similar values, $(148 \pm 7, 110 \pm 5, 92 \pm 4)$ km s^{-1}, so it appears that the shape of the velocity ellipsoid remains essentially unchanged with varying [Fe/H] below [Fe/H] = −1.7. In this regard Norris (1994) claimed, from his analysis of a sample of high proper-motion stars, that σ_W continues to increase with decreasing [Fe/H], even at its lowest levels. This result was taken to indicate the possible existence of a dynamically "hot" proto-disk population at low abundances. Carney et al. (1996) disputed this result, as their analysis of a different set of high proper-motion stars indicated that the disk component is not dynamically hot, at least when membership is confined to the stars orbiting exclusively within the inner part of the Galaxy, $R \leq 14$ kpc. Figure 2c shows no evidence for an increase of σ_W at low abundances.

The velocity dispersion components of the Selected Sample in the more metal-rich abundance ranges decrease as the contribution of the thick disk component progressively increases. In particular, for $-0.7 \leq$ [Fe/H] < -0.6 and $|Z| < 1$ kpc, where the contribution of the halo

component is expected to be negligible, the mean V velocity, $< V >$, is -20 ± 5 km s^{-1}; the velocity dispersions are $(\sigma_U, \sigma_V, \sigma_W) = (46 \pm 4, 50 \pm 4, 35 \pm 3)$ km s^{-1} . This result is in agreement with previously derived kinematic parameters for the thick disk, which appears to be in rapid rotation ($\sim$200 km s^{-1}), provided the rotational speed of the LSR is $V_{LSR} = 220$ km s^{-1} (BSL). With these values for the thick disk kinematics, it is possible to estimate the radial scale length of this component using the following formula (Binney & Tremaine 1987):

$$2V_{LSR}V_{lag} - V_{lag}^2 = \sigma_U^2 \left(-1 + \frac{\sigma_V^2}{\sigma_U^2} + 2\frac{R}{h_R} \right) , \quad (1)$$

where V_{lag} is the asymmetric drift given by $V_{lag} = - < V >$, and h_R is the scale length of the disk, provided its density varies as $\exp(-R/h_R)$. By inserting $V_{LSR} = 220 \pm 10$ km s^{-1}, the assumed solar radius $R = 8.5$ kpc (Kerr & Lynden-Bell 1986) and derived parameters for $-0.7 \leq$ [Fe/H] < -0.6 in Equation (1), we obtain $h_R = 4.5 \pm 0.6$ kpc. This is in good agreement with $h_R = 4.7 \pm 0.5$ kpc obtained by BSL, and also with the lower limit of $h_R \simeq 4.5$ kpc derived by Ratnatunga & Freeman (1989). We note that the second term on the left-hand side of Equation (1) has been omitted in some previous works, as it is small compared to other terms. If we were to exclude this term, we would obtain $h_R = 4.3 \pm 0.6$ kpc, thereby slightly underestimating h_R.

2.2. Rotational Character of the Selected Sample

We now examine the rotational character of the Selected Sample. Figure 3 shows the mean rotational velocities $< V_\phi >$ (the rotation velocity in a cylindrical coordinate frame) as a function of [Fe/H], based on stars in the Selected Sample. The left-hand panel in Figure 3a displays the results for the abundance ranges listed in Table 2, for three subsets of the sample as a function of distance above the plane. In the right-hand panel of Figure 3a, the bins are obtained by passing a box of width $N = 100$ stars, ordered by metallicity, with an overlap of 20 stars each. The latter approach is adopted to avoid any effects of the arbitrary placement of bins on the results.

Note that the panels in Figure 3a are obtained with full knowledge of the space motions of the stars in the Selected Sample. Figure 3b is based on the radial velocities alone, applying the methodology of Frenk & White (1980) (FW) (see also Norris 1986; Morrison, Flynn, & Freeman 1990, hereafter MFF; BSL). The solid lines in the left and right-hand panels of Figure 3b denote $< V_\phi >$ as derived for the stars with available proper motions (denoted as $< V_\phi >_{pm}^{FW}$ in Table 2), i.e., the same sample as in Figure 3a, whereas the dashed lines are for all of the stars with available radial velocities ($< V_\phi >_{all}^{FW}$ in Table 2). Comparison between Figures 3a and 3b allows us to examine whether the Selected Sample is subject to any significant kinematic bias, since, if so, the $< V_\phi >$ derived from the space motions is expected to be systematically smaller from that determined on the basis of radial velocities alone (Ryan & Norris 1991; Norris & Ryan 1991).

Figure 3a clearly indicates that the rotational properties of the Selected Sample change

discontinuously at [Fe/H] $\simeq -1.7$. Stars with [Fe/H] < -1.7 exhibit no systematic variation of $< V_\phi >$ with decreasing [Fe/H]. It is interesting to note that the subsample of low-abundance stars with $|Z| < 1$ kpc show a rather large prograde rotation of $< V_\phi >= 30 \sim 50$ km s^{-1}, and that $< V_\phi >$ decreases if stars at larger heights are considered, at least for the two abundance bins centered on [Fe/H] $= -1.9$ and -2.2, respectively. This behavior is not exhibited, however, for stars in the lowest abundance bin. To check the significance of this feature, we have combined the stars in our Selected Sample in the metallicity interval $-2.4 \leq$ [Fe/H] ≤ -1.9 and obtained $< V_\phi >$ by sweeping a box of 50 stars ordered by $|Z|$, with an overlap of 30 stars. The results are summarized in Table 3 and depicted in Figure 4. The lower solid line in Figure 4 is a least-squares fit to the data, which yields $\Delta < V_\phi > /\Delta|Z| = -52 \pm 6$ km s^{-1} kpc^{-1}, indicating the presence of a significant vertical gradient in $< V_\phi >$ at low abundances. Figure 4 also suggests that $< V_\phi >$ beyond $|Z| \sim 1.2$ kpc has a nearly constant zero value. If we exclude the last point at $|Z| = 1.76$ kpc from the fit, we obtain $\Delta < V_\phi > /\Delta|Z| = -62 \pm 5$ km s^{-1} kpc^{-1} (shown as a dotted line). Note that Majewski (1992) reported evidence for a halo component which is in retrograde motion ($V_\phi = -275 \pm 16$ km s^{-1}), but which exhibited no gradient of rotation with distance from the plane, a result that is clearly at odds with our present result.

Figure 3a shows that for stars in the Selected Sample with [Fe/H] > -1.7 there is a clear linear dependence of $< V_\phi >$ on [Fe/H], a dependence that remains essentially unchanged even if the range of $|Z|$ is varied. This discontinuity has been seen before, of course, based on analysis of smaller samples (e.g., Norris 1986; Carney 1988; Zinn 1988; Norris & Ryan 1989; BSL; CY). The inescapable conclusion is that the transition from halo to disk must not have occurred in a continuous manner, as predicted in the ELS model. However, the vertical gradient in $< V_\phi >$ for metal-poor stars noted above suggests that the halo was not formed in a totally chaotic, dissipationless manner as implied in the SZ hypothesis. Rather, dissipational processes may have played a role in the initial contraction of the halo, likely involving energy exchange with the gas phase (Carney et al. 1996).

It is also worth noting from Figure 3 that the stars of the thick disk, which dominate the Selected Sample for [Fe/H] > -1, exhibit only a small change in $< V_\phi >$ with increasing $|Z|$. Table 3 and Figure 4 summarize the change of $< V_\phi >$ with $|Z|$ for stars likely to be dominated by the thick disk, i.e., in the abundance range $-0.8 \leq$ [Fe/H] ≤ -0.6. The least-squares fit to the data (as shown by upper solid line) yields $\Delta < V_\phi > /\Delta|Z| = -30 \pm 3$ km s^{-1} kpc^{-1}, much smaller than the gradient obtained for halo stars with $-2.4 \leq$ [Fe/H] ≤ -1.9, but similar to previous estimates of the thick disk rotational velocity gradients reported by Majewski (1992).

The relation between $< V_\phi >$ and [Fe/H] as shown in the panels of Figure 3a is also seen in the panels of Figure 3b. In particular, $< V_\phi >$ obtained from the subsample having available proper motions (dashed lines) is essentially the same as that from the entire sample (solid lines) within standard errors in $< V_\phi >$ (except for [Fe/H] ~ -1.6: see below). This is consistent with our argument given in Paper II that the subsample based on stars with available proper motions is not subject to any significant kinematic bias.

We note that near [Fe/H] = −1.6 in Figure 3b, $< V_\phi >$ obtained from consideration of the sample with full space motions is *larger* than that obtained from the sample using radial velocities alone. The apparent retrograde rotation of globular clusters in the similar metallicity range was also reported by Rodgers & Paltoglou (1984) based on radial velocities alone, whereas Dinescu, Girard, & van Altena (1999) found no sign of significant retrograde rotation using full space motions of globular clusters. It is worth noting that this difference in the rotational velocity using either of radial velocities or full space motions is not a signature of kinematic bias, since the result is in the opposite direction to that expected. This difference probably arises due to limitations of the FW methodology as applied to our sample. The FW method implicitly assumes that the angle, ψ, between the line-of-sight and the rotational direction is randomly distributed in the sample, which may not apply in this case. In addition, the apparent excursion to large retrograde rotation, $< V_\phi > \simeq -40$ km s^{-1} near [Fe/H] = −1.6 in the right-hand panel of Figure 3b (also noted by BSL), may be caused by a few outliers having large velocities as seen by an observer at rest with respect to the Galactic center, V_{gal}. If we exclude five stars having large V_{gal} from the bin centered at [Fe/H] = −1.6, we obtain $< V_\phi > = -12$ km s^{-1}. We have verified that the effect of outliers on $< V_\phi >$ is small in other abundance ranges.

The influence of a disk-like population for [Fe/H] > −1.7 is certainly suggested by the appearance of Figure 3. The question of the limiting abundance of a so-called metal-weak thick disk (MWTD)[1] has been considered several times in the past (MFF; Rodgers & Roberts 1993; Layden 1995; BSL; Ryan & Lambert 1995; Twarog & Anthony-Twarog 1996; CY). Figure 5 shows the frequency distribution of V_ϕ for the stars in the Selected Sample with available space motions, for subsets chosen to have (a) $|Z| < 1$ kpc, and (b) $|Z| \geq 1$ kpc, respectively. At $|Z| < 1$ kpc, where the disk-like kinematics are expected to be more evident than at larger heights above the plane, the metal-rich stars with [Fe/H] > −1 are peaked at $V_\phi = 200$ km s^{-1}, a rather high rotational velocity. One also sees the presence of a small contribution of the stars with halo-like kinematics. At lower abundances the halo-like kinematics become much more dominant; the contribution of the MWTD is apparently decreasing at lower abundances and higher $|Z|$.

To quantify the fraction of the MWTD in our local sample within the specified abundance ranges, we have fit the subset of stars with $|Z| < 1$ kpc using a mixture of two Gaussian distributions for V_ϕ, representing the halo and disk populations. The halo kinematic parameters $(< V_\phi >_{halo}, \sigma_{\phi,halo}) = (+33,106)$ km s^{-1} are derived from stars with [Fe/H] ≤ −2.2. The rotation velocity of the disk component, $< V_\phi >_{disk} = +200$ km s^{-1}, is obtained considering the stars in the metallicity range $-0.7 <$ [Fe/H] ≤ -0.6. With these parameters fixed, we evaluate the most likely values of the velocity dispersion of the disk, $\sigma_{\phi,disk}$ and fraction F of the MWTD, using a maximum likelihood analysis (see also MFF; CY). The likelihood function for the stars with V_ϕ^i is given by

[1]These metal-poor stars with disk-like kinematics may also include a considerable portion of the thin disk if its metallicity distribution overlaps that of the thick disk (Wyse & Gilmore 1995).

$$\log f(F, \sigma_{\phi,disk}) = \sum_{i=1}^{N} \log[F f^i_{disk} + (1-F) f^i_{halo}] \ , \qquad (2)$$

where f^i_{disk} (f^i_{halo}) denote Gaussian functions with mean velocities $< V_\phi >_{disk}$ ($< V_\phi >_{halo}$) and dispersions $\sigma_{\phi,disk}$ ($\sigma_{\phi,halo}$). The results of the likelihood analysis are tabulated in Table 4, and shown by the solid curves in Figure 5. The MWTD contributes about 30% of the metal-poor stars in the abundance range $-1.7 <$ [Fe/H] ≤ -1, which is smaller than the fraction derived by MFF ($\sim$72%) and BSL ($\sim$60%), but larger than the result of CY ($\sim$10%). The fraction of the MWTD is quite modest in the more metal-poor ranges, in contrast to the suggestion of BSL, who argued for $\sim$30% even at [Fe/H] < -2. One reason that our result may differ so strikingly from that of BSL is that the estimated abundances for many of the HK survey stars at [Fe/H] < -2, listed in the original BSL catalog, are likely to have been underestimated by ~ 0.3 dex (see Figure 1 of Paper II).

The RR Lyrae stars in our Selected Sample (shown as shaded histograms in Figure 5) exhibit no clear disk-like kinematics, even in the intermediate abundance range of $-1.7 <$ [Fe/H] ≤ -1. This confirms earlier results by MFF, Layden (1995), and CY, and may imply a somewhat younger age of the thick disk as compared to the halo. However, the numbers of RR Lyraes with available space motions is rather small, so this question, especially in conjunction with their period distributions to investigate different populations of RR Lyraes (Lee & Carney 1999), should be revisited when the sample size has been increased.

3. Orbital Properties of the Metal-Poor Stars

In this section we investigate the orbital properties of our sample of stars in a given Galactic potential. We adopt the analytic Stäckel-type potential developed by Sommer-Larsen & Zhen (1990, hereafter SLZ), which consists of a flattened, oblate disk and a nearly spherical massive halo. This model potential is consistent with the mass model of Bahcall, Schmidt, & Soneira (1982), exhibiting a flat rotation curve beyond $R = 4$ kpc, and having a commensurate local mass density at $R = R_\odot$. In contrast to a non-analytic potential, for which numerical integrations of orbits are required, the analytic nature of the adopted potential has the great advantage of maintaining clarity in the analysis, as demonstrated below. In the Appendix, we summarize the properties of the Stäckel mass model, and provide expressions for three integrals of motion in such a model (see also de Zeeuw 1985; Dejonghe & de Zeeuw 1988)

3.1. The Relationship between Orbital Eccentricity and Metal Abundance

We first compute orbital eccentricities, defined as $e = (r_{ap} - r_{pr})/(r_{ap} + r_{pr})$, where r_{ap} and r_{pr} denote the apogalactic and perigalactic distances of the orbits, respectively. These orbital

parameters are tabulated in Table 3 of Paper II for the stars under consideration. In Figure 6a, we show the relation between e and [Fe/H]. As is evident, there is *no strong correlation* between these quantities, and the metal-poor stars below [Fe/H] = −2 exhibit a diverse range in orbital eccentricities. This is in sharp contrast to the ELS result, and confirms previous suggestions from a number of workers, but in a much more definitive manner (Yoshii & Saio 1979; NBP; Carney & Latham 1986; Carney, Latham, & Laird 1990; Norris & Ryan 1991; CY). In addition to the diverse distribution of e at all abundances, we note a small concentration of the stars at $e \sim 0.9$ and [Fe/H] ~ -1.7, which is somewhat reminiscent of the original ELS result. It is perhaps not coincidental that the excess number of high-e stars occurs at an abundance which matches the sharp discontinuity of $< V_\phi >$ found at [Fe/H] = −1.7, where $< V_\phi >$ is almost zero (Figure 3). This may suggest that a significant fraction of the metal-poor stars with abundances near [Fe/H] = −1.7 formed from infalling gas of this metallicity during an early stage of Galaxy formation, in a manner similar to an ELS collapse.

In Figure 6b, we show the mean eccentricity, $< e >$, vs. [Fe/H], where the bins are obtained by passing a box of width $N = 100$ stars, ordered by metallicity, with an overlap of 20 stars each. For comparison, the dashed line denotes the result of Carney et al. (1996) for their high proper motion sample. There is a clear difference from our results – the use of a kinematically selected sample *overestimates* the average orbital eccentricities at a given [Fe/H], by an amount up to 0.2.

Figure 7 shows the cumulative distributions of e, $N(< e)$, in two specific abundance ranges, (a) for [Fe/H] ≤ -2.2, and (b) for $-1.4 <$ [Fe/H] ≤ -1. Figure 7a clearly demonstrates that even at quite low abundance, roughly 20% of our stars have $e < 0.4$. The different lines correspond to the cases when the range of $|Z|$ is changed. It is apparent that, for stars with [Fe/H] ≤ -2.2, the cumulative distribution function of e is unchanged when considering subsets of the data with a range of $|Z|$, suggesting the absence of any substantial disk-like component below this metallicity. By way of contrast, Figure 7b shows that stars with intermediate abundances exhibit (a) a higher fraction of orbits with $e < 0.4$ than for the lower abundance stars, (b) a decrease in the relative fraction of low eccentricity stars as larger heights above the Galactic plane are considered, and (c) convergence at larger heights to a fraction which is close to the 20% obtained for the lower abundance stars. These results imply that the orbital motions of the stars in the intermediate abundance range are, in part, affected by the presence of thick-disk component with a finite scale height. We recall that CY and Chiba, Yoshii & Beers (1999), using a sample of metal-poor stars with *Hipparcos* measurements, found a further decrease of the fraction of the stars with $e < 0.4$ at larger $|Z|$, without achieving the convergence noted here (see Figure 15 of CY). This was presumably due to the lack of a sufficient number of intermediate abundance stars at large $|Z|$ in the sample considered by these authors.

3.2. Structural Parameters of the MWTD Component

We now seek to quantitatively describe the abundance range, scale height, and fraction of the MWTD component in our sample. We apply a Kolmogorov-Smirnoff (KS) test of the null hypothesis that the differential distributions of e, $n(e)$, for stars in a specified abundance range, are drawn from the same parent population of eccentricities as stars belonging to a "pure" halo component. Based on our analysis above, we take the subsample of 78 stars with [Fe/H] ≤ -2.2 and $|Z| < 1$ kpc to represent the pure halo component. We then calculate the KS probabilities, P_{KS}, for the stars in various intermediate abundance ranges and with $|Z| > Z_{lim}$, where Z_{lim} is the lower limit on the heights of the stars above the Galactic plane. We expect that, even if the specified abundance range is contaminated by stars with disk-like kinematics, it will be dominated by halo-like kinematics above *some* $|Z| = Z_{lim}$, with P_{KS} exceeding 0.2 (i.e., the subsamples being consistent with draws from the same parent population of orbital eccentricities).

Figure 8 shows the results of the KS tests. In order to obtain an estimate for the value of Z_{lim} above which the populations cannot be distinguished, Figure 8a depicts the results for the stars below [Fe/H] $= -1$, but above the specified *lower limit* for the abundance. In the left-hand panel of Figure 8a, it is seen that P_{KS} rapidly increases at $Z_{lim} = 0.5$ to 1.3 kpc and then remains roughly constant at larger Z_{lim}. In the right-hand panel of Figure 8a, the distribution of P_{KS} on Z_{lim} changes dramatically as one passes from the inclusion of stars with [Fe/H] > -1.9 to those with [Fe/H] > -2.0. When stars with abundances as low as [Fe/H] $= -2.0$ are included, there is *no value* of Z_{lim} for which the distributions can be distinguished. To identify the lower limit on the abundance of stars which are members of the MWTD, Figure 8b shows the distribution of P_{KS} for metal-poor stars above [Fe/H] $= -2.2$, but below the specified *upper limit* on abundance. As is seen in the left-hand panel of this figure, P_{KS} remains small (indicating that the populations can be distinguished) at all Z_{lim}. In the right-hand panel of Figure 8b, one sees that although there exists a region at small Z_{lim} where the populations can be marginally distinguished when the upper limit on abundance is taken to be [Fe/H] $= -1.9$, there is no such region when stars with an upper limit of [Fe/H] $= -2.0$ is considered. These results suggest that the MWTD component has a characteristic scale height of roughly 1 kpc, above which halo-like orbital motions dominate, and a lower abundance limit near [Fe/H] $= -2.0$. We note here that the number of stars employed in the KS tests is sufficiently large in the ranges of Z_{lim} considered (e.g. $N = 240$ for $-2 <$ [Fe/H] ≤ -1 and $N = 54$ for $-2.2 <$ [Fe/H] ≤ -2 at $Z_{lim} = 1$ kpc). However, it would be useful, especially at larger Z_{lim}, to boost the sample sizes so that more detailed investigations can be carried out.

We now estimate the contribution of the MWTD component in the solar neighborhood, F, using the distribution of e in various abundance ranges. Following the methodology developed by CY, we perform a Monte Carlo simulation to predict the e-distribution from a mixture of stars contributed by the thick-disk and halo populations, adopting the kinematic parameters for these components derived in §2, and compare with the observed cumulative distribution functions of eccentricity in our sample with $|Z| < 1$ kpc. Figure 9 shows the results of this exercise. As is clear,

more metal-rich ranges are described by a larger F, but in the abundance range $-2.2 <$ [Fe/H] ≤ -2, $F \simeq 0$, in good agreement with the results obtained from comparison of the differential eccentricity distributions. Figure 10 shows the dependence of F on [Fe/H] for stars with $|Z| < 1$ kpc, where the fits are made with bins of 0.2 dex for [Fe/H] and 0.1 for F. The F([Fe/H]) derived here, based on full knowledge of the stellar orbital motions, is rather similar to that found by BSL based on radial velocities alone, except for the abundance range below [Fe/H] < -1.5, where the MWTD appears more modestly populated. A characteristic value of $F = 0.3$ over the abundance range $-1.7 <$ [Fe/H] ≤ -1 is obtained from our present analysis.

Having obtained the structural parameters of the MWTD component, we extract a set of likely members of the MWTD component in our sample. High-resolution spectroscopic observations of these stars, to obtain estimates of their individual elemental abundances, should provide valuable information concerning the nature of MWTD stars, and reveal differences, if any, in their compositions relative to similar metallicity stars of the halo population (e.g., Bonifacio, Centurion, & Molaro 1999). In Table 5 we list the stars satisfying (1) $-2.2 \leq$ [Fe/H] ≤ -1, (2) $|Z| \leq 1$ kpc, (3) $V_\phi \geq < V_\phi >_{disk} - \sigma_{\phi,disk}$, and (4) $|V_R| \leq \sigma_{R,disk}$ and $|V_Z| \leq \sigma_{Z,disk}$, where $< V_\phi >_{disk} = 200$ km s^{-1} and $(\sigma_{R,disk}, \sigma_{\phi,disk}, \sigma_{Z,disk}) = (46, 50, 35)$ km s^{-1}, as derived above). Condition (3) corresponds to the high rotation velocity of the candidate members and condition (4) is placed so that their velocities in R and Z directions are confined within a 1 σ range relative to the zero mean, i.e. within the velocity dispersions of the MWTD component. In Table 5, the fourth column denotes the classification of each stellar type. We follow the coding of paper II – D: main-sequence dwarf star; TO: main-sequence turnoff star; SG: subgiant star; G: giant star; AGB: asymptotic giant branch star; FHB: field horizontal-branch star; RRV: RR Lyrae variable star; V: variable star. Note that Table 5 supersedes Table 8 of BSL, as we now have much more complete kinematic information.

4. Global Dynamics and Structure of the Halo

Although our present sample is dominated by stars located in the vicinity of the Sun, the orbits of many of these stars explore regions well into the more distant halo of the Galaxy. Thus, their local kinematics provide information on the global dynamics and structure of the halo (May and Binney 1986). In this section we first investigate the rotational properties of the halo at large heights from the Galactic plane, then use this same sample to obtain a picture of the global density distribution of the halo.

4.1. Rotational Properties of the Halo

Majewski (1992) claimed, on the basis of measured proper motions for an *in situ* sample of halo subdwarfs located at $Z > 5$ kpc (in a small field in the direction of the North Galactic

Pole), that stars at such large heights above the Galactic plane exhibit a net *retrograde* rotation $< V_\phi > \simeq -55 \pm 16$ km s^{-1}, in contrast to the stars nearer the plane, which show a near-zero or slightly prograde rotation. Although there have been criticisms of this result (e.g., Ryan 1992), a number of workers have also reported observations of separate samples which seem to support this view, so the true situation has remained unclear. For example, Carney et al. (1996) reported evidence for a retrograde rotation in the subset of their local sample of high proper-motion stars whose orbits extend far above the plane. In their analysis, they divided the sample into those stars with $Z_{max} \leq 2$ kpc, and $Z_{max} \geq 5$ kpc, respectively, where Z_{max} is the maximum distance of the derived orbit from the plane. Carney et al. showed that their "high halo" sample, with < [Fe/H] >= −2.04 and $Z_{max} \geq 5$ kpc, exhibited a net retrograde rotation ($< V_\phi >= -45 \pm 22$ km s^{-1}), whereas their "low halo" sample at $Z_{max} \leq 2$ kpc exhibited a net prograde rotation ranging from $< V_\phi >= 12$ km s^{-1} to 44 km s^{-1}, depending on the specific criteria chosen to avoid stars of the disk component.

Figure 11a reproduces the original data of Carney et al. (1996), for stars with [Fe/H] ≤ −1.5. Since, in their estimates of Z_{max}, Carney et al. adopted a different Galactic potential than ours, we have also re-determined Z_{max} for their sample with the same potential described in §3, and show the results in this same figure. Regardless of the adopted potential, it is apparent that the stars at $Z_{max} \geq 5$ kpc exhibit a net retrograde rotation, as compared to the stars at $Z_{max} \leq 2$ kpc, which are in prograde rotation. Carney et al. argued that this result might be explained by the presence of two distinct halo populations, a high halo formed via accretion of fragments (such as in the SZ model), and a low halo formed from an organized contraction (similar to the ELS model).

The Carney et al. sample is based on high proper-motion stars selected from the Lowell Proper Motion Catalog, where proper motions are measured to exceed 0.26" yr^{-1}, and the New Luyten Two-Tenths Catalog with proper motions exceeding roughly 0.18" yr^{-1}. Thus, their sample is *a-priori* biased against inclusion of stars with prograde rotation close to the velocity of the LSR. What remains to be evaluated is the effect that this kinematic bias may have on the observed kinematics of the high halo.

We consider the question of bias in the Carney et al. sample via a Monte Carlo simulation, with the following assumptions. "Stars" with [Fe/H] < −1.5 are randomly distributed in Galactic coordinates (l, b), and are assumed to have a Gaussian velocity distribution with $(\sigma_U, \sigma_V, \sigma_W) = (141, 108, 94)$ km s^{-1}, but with no systematic rotation. Distances to the simulated stars are taken by adopting a Gaussian form with mean 0.18 kpc and dispersion 0.09 kpc, which reproduces well the distance distribution of their sample stars. We further assume that only the stars whose inferred proper motions exceed 0.26" yr^{-1} are observed at the Sun with $V_{LSR} = 220$ km s^{-1}. The result is shown in panel Figure 11b. The simulated data sample exhibits a net retrograde rotation for stars in the high halo. We note that our simulation does *not* exhibit a net prograde rotation in the low halo, as seen in the Carney et al. sample. This may arise because their sample is not distributed randomly in (l, b), as our simulation assumes, and/or because their

disk sample may be mainly drawn from stars for which the proper motion limit is 0.18" yr^{-1}. Nevertheless, the results of this simple simulation provide reason to be skeptical of their claim of the existence of a retrograde high halo, which clearly *can* be influenced by selection bias of the input sample[2].

Our large non-kinematically selected sample provides the means to elucidate the rotational character of the high halo without the effect of an input selection bias. Figure 11c presents our results based on sample stars with [Fe/H] ≤ -1.5. It is found that the stars at small Z_{max} show a net prograde rotation, in agreement with the results presented in §2 and also with the Carney et al. (1996) result: we obtain $< V_\phi >= 59 \pm 7$ km s^{-1} for 230 stars at $Z_{max} < 2$ kpc. However, at large Z_{max}, the stars exhibit *no systematic rotation*, in sharp contrast to the Carney et al. result: we obtain $< V_\phi >= 0 \pm 8$ km s^{-1} for 212 stars at $Z_{max} \geq 4$ kpc. We note that although there is a difference in the rotational velocities for the stars close to and farther from the plane, which may suggest two populations (accreted and contracted populations), the boundary between them is not obvious.

4.2. The Global Density Distribution of the Halo

May & Binney (1986) discussed the interesting possibility that, on the basis of Jeans' theorem, the *global* structure of the stellar halo can be recovered from *local* kinematic information for a sufficiently large sample of stars observed in the solar neighborhood. The theorem states that, for a well-mixed stellar system, the six-dimensional phase-space distribution function of stars, $f(\mathbf{x}, \mathbf{v})$, can be taken to be a function of the three isolating integrals of motion I_i, $i = 1, 2, 3$, i.e. $f(I_1, I_2, I_3)$. Within this isolating integral space, the stars constitute a set of fixed points with no time evolution. May & Binney argued that the stars observed in the solar neighborhood actually occupy a large fraction of this phase space, and it is hence possible to reconstruct the global structure of the stellar system from the kinematic data of nearby stars. Following these strategies, SLZ developed a maximum likelihood method for recovering a global model of the halo based on a discrete sum of orbits, and applied it to a sample of 118 local stars with [Fe/H] ≤ -1.5 selected without kinematic bias. SLZ found that the stellar halo at $8 < R < 20$ kpc may consist of two components – a main, nearly spherical component, and an overlapping, highly flattened component. We note here that the *actual* halo system is unlikely to be in a well mixed equilibrium state, as we will discuss in the next section. However, the relaxation process is very slow compared to the orbital periods of typical stars, so the Jeans theorem and the above approach based on it are at least approximately valid.

We now apply the SLZ methodology to the present sample of stars, which is both larger, and

[2]Carney (1999) reported that, after making a statistical correction for the kinematic bias in the Carney et al. 1996 sample, he also obtained a net prograde rotation even in the high halo.

has more accurately determined kinematic information than was available to SLZ. To exclude the MWTD stars as much as possible, we select as representatives of the halo population the stars in our sample with [Fe/H] ≤ -1.8, a more restrictive abundance cut than the [Fe/H] ≤ -1.5 used by SLZ. We also select a sample of stars with $-1.6 <$ [Fe/H] ≤ -1 in order to examine the characteristics derived for a halo population contaminated by the MWTD. To minimize the effects of distance errors we limit our samples to those stars satisfying $D \leq 4$ kpc. We also remove stars with inferred (and possibly incorrect) extreme space motions ($V_{RF} \leq 550$ km s^{-1}). After applying these cuts, the samples we investigate include $N = 359$ stars for [Fe/H] ≤ -1.8, and $N = 302$ stars for $-1.6 <$ [Fe/H] ≤ -1 .

The method is summarized as follows (see SLZ for the complete description): (1) the N sets of isolating integrals $(I_{1,i}, I_{2,i}, I_{3,i})$, $i = 1, ..., N$ are calculated from the observed positions $\mathbf{x}_i$ and velocities $\mathbf{v}_i$ of the stars, within an assumed Galactic potential. Here, I_1 is the total orbital energy E, I_2 is proportional to the square of the angular momentum vector pointing in the Z-direction $I_2 = L_z^2/2$ (which measures azimuthal angular momentum), and I_3 is the so-called third integral of motion as defined in the Appendix (see also equation 15 of SLZ). For the Galactic potential, we adopt the same Stäckel model as in §3. (2) At all locations of the stars $\mathbf{x}_j$, $j = 1, ..., N$, the probability density $\rho_i(\mathbf{x}_j)$ of an orbit characterized by $(E_i, I_{2,i}, I_{3,i})$ is calculated for $i = 1, ..., N$. In other words, we calculate the N^2 matrix ρ_{ij}, $i, j = 1, ..., N$ from knowledge of integrals and locations of the orbits. (3) By maximizing the probability that the star found at $\mathbf{x}_{j=1}$ is on orbit $i = 1$, the star found at $\mathbf{x}_{j=2}$ is on orbit $i = 2$, and so forth, the orbit weighting factors, c_i, are used to estimate the total density at $\mathbf{x}$, viz

$$\rho(\mathbf{x}) = \sum_{i=1}^{N} c_i \rho_i(\mathbf{x}) \ . \tag{3}$$

Thus, equation (3) provides an estimate of the density of the halo stars at any point $\mathbf{x}$. The method also permits one to derive the mean azimuthal velocities as:

$$< V_\phi > (\mathbf{x}) = \frac{1}{\rho(\mathbf{x})} \sum_{i=1}^{N} c_i \rho_i(\mathbf{x}) V_{\phi,i}(\mathbf{x}) \ . \tag{4}$$

We proceed to average the results from equations (3) and (4) over grids of finite area. Following SLZ, we define the grids in the meridional plane of the spheroidal coordinates (λ, ν), which is a suitable choice for Stäckel mass models (see the Appendix for more details). The grids are defined as $\lambda_k = k^2 - \alpha$, $k = 1, ..., 30$ and $\nu_l = (\gamma - \alpha)\cos^2(\theta_l) - \gamma$, $\theta_l = (\pi/2)(l/20)$, $l = 0, ...20$, as shown in Figure 4 of SLZ, where α and γ are constants. The spatial resolution of the grids is about 1 kpc.

Figure 12a shows a plot of the reconstructed density distribution at the Galactic plane (the averaged density over the area at $l = 20$), for [Fe/H] ≤ -1.8 (filled circles) and $-1.6 <$ [Fe/H] ≤ -1 (open circles). As a comparison, the results using the SLZ sample with [Fe/H] ≤ -1.5 are also shown (crosses). As in the analysis of SLZ, the density distribution for $R > 8$ kpc is well described by a power-law model $\rho \propto R^\beta$. For [Fe/H] ≤ -1.8, we find that the power-law model

with exponent $\beta = -3.55 \pm 0.13$ fits well at all radii beyond $R = 8$ kpc, up to the grid point for the largest radius, $R = 35$ kpc. Note that for the SLZ sample the density at the largest three radii appears to fall short of the power-law model (probably as a result of their smaller sample size). If we omit these outer points, we obtain a fit to the power-law index $\beta = -3.57 \pm 0.16$ at $8 < R < 28$ kpc, which is yet slightly steeper than the $\beta = -3.29$ result of SLZ. It is of interest to note that a power-law model with exponent $\beta \simeq -3.5$ derived for our sample of field halo stars is similar to the radial density distribution of the halo globular cluster population derived by Harris (1976) and Zinn (1985) ($\beta = -3.5$) and by Carney, Latham, & Laird (1990) ($\beta = -3.0$). A similar density distribution, but with a slightly shallower slope, has been found for field RR Lyrae stars by Saha (1985) ($\beta \simeq -3$) and Hawkins (1984) ($\beta \simeq -3.1$). Preston et al. (1991) combined counts of RR Lyrae stars and FHB stars in several fields to obtain the exponent $\beta = -3.5 \pm 0.3$. We see, in our reconstructed density distribution, no clear evidence for a break in the density distribution at $R = 20 - 25$ kpc as was detected in the number counts of globular clusters and RR Lyraes. For the subsample of stars with $-1.6 <$ [Fe/H] ≤ -1, we obtain $\beta = -3.47 \pm 0.18$ for $8 < R < 25$ kpc, thus contamination from the MWTD has little effect. Below $R = 8$ kpc, the density distributions of all three samples clearly deviate from a single power-law model, a result which is likely caused by incomplete representation, in the solar neighborhood, of stars for which apocentric radii are below $R = R_\odot$.

Figure 12b shows the mean azimuthal velocities, $< V_\phi >$, for the same three samples of stars, projected onto the Galactic plane. The value of $< V_\phi >$ is nearly zero for $R > 10$ kpc, but there is a signature of *increasing* $< V_\phi >$ with decreasing R. In particular, for the sample of stars with $-1.6 <$ [Fe/H] ≤ -1, $< V_\phi >$ rises rather discontinuously at $R \simeq 10$ kpc, which may correspond to the radial limit of the rapidly rotating thick-disk component.

Figure 13 is a plot of the inferred global density distribution in the (R, Z) plane, in the form of equidensity contours. The lack of stars at small R and large Z (which gives rise to the ill-formed contour levels in this portion of the diagram) is a consequence of the small probability that stars in the Galaxy that explore such a region are represented in the solar neighborhood (as argued in SLZ). Other than in this region, the inferred density distribution based on the 359 stars with [Fe/H] ≤ -1.8 (panel b) appears to be very similar to that which SLZ obtained from their 118 stars (panel a): The outer part of the halo, at $R > 15$ kpc, is round, in good agreement with inferences based on star counts (see Freeman 1987 and references therein; Preston et al. 1991).

While we reproduce the general sense of the SLZ results with our much larger sample, there are notable differences in the details. SLZ argued that there is a clear indication that the halo, at any given radius, consists of *both* a main, nearly spherical component and an *overlapping*, highly flattened component. There no clear evidence for this result in the density reconstruction based on our new data. To further examine this point, we have fit elliptical contours to the reconstructed density maps after, following SLZ, *omitting* the data points near the Galactic plane. Specifically, we obtain fits to ellipses of major axis a, and axial ratio q, over the polar angle $40° < \theta < 80°$. Residuals to the fits obtained to these ellipses as a function of polar angle are shown in Figure

14a. Thick solid and dotted lines correspond to the fits with $a = 10.5$ kpc and $q = 0.70$ and with $a = 13.5$ kpc and $q = 0.51$, respectively, for our sample with [Fe/H] ≤ -1.8. For comparison, we show the corresponding results using the SLZ sample fit over $30^\circ < \theta < 80^\circ$ (thin solid and dotted lines). It follows that, while we reproduce the SLZ result that there is a large density excess near the Galactic plane when using *their* sample, it is not evident in *our* sample – an additional flat component is not required for the fitting.

Based on the above result, we proceed to make a fit including the density data near the plane, with a single value for the axial ratio q at each major axis a, i.e., without taking into account an additional flat component having small q. The change of our estimate of q as a function of radius is shown in Figure 14b. For the sample of stars with [Fe/H] ≤ -1.8, the density distribution in the outer part of the halo, $R \sim 20$ kpc, is quite round. However, the axial ratio q appears to decrease with decreasing R over $15 < R < 20$ kpc, and the inner part, at $R < 15$ kpc, exhibits $q \sim 0.65$. Thus, the halo can be described as nearly spherical in the outer part and highly flattened in the inner part, instead of the overlap of both components at all locations in the halo. This result is in good agreement with previous studies of the distribution of RR Lyrae (Hartwick 1987; Layden 1995) and FHB stars (Preston et al. 1991; Kinman, Suntzeff, & Kraft 1994), as well as with the flattening of the inner halo reported by Larsen & Humphreys (1994) based on counts of F- and G-type stars. It remains an open question as to whether or not there exists a distinct boundary between the outer spherical halo and the inner flattened halo.

As seen in Figure 13c, the density distribution in the inner part of the halo for stars of intermediate abundance ($-1.6 <$ [Fe/H] ≤ -1) appears to be more flattened than is the case for stars with [Fe/H] ≤ -1.8. This result is reflected in the ellipse fits for these stars shown in Figure 14b, which indicate that $0.5 < q < 0.6$ at $R < 12$ kpc. This may be due to the contribution of the (by definition) flattened, MWTD population with a finite radial scale length. We note that our results imply the decrease of axial ratios at $R > 17$ kpc. This may be an artifact due to the small numbers of stars employed at such large radii, so further analysis using much larger samples is necessary.

5. Kinematic Substructure of the Halo in the Solar Neighborhood

If the halo of the Galaxy was assembled from the merging and/or accretion of small subgalactic clumps, as argued by SZ, then one might hope to find signatures of those events, even now, in the form of kinematic substructures, because the mixing of phase space for such stars is expected to be incomplete (Helmi & White 1999). The Sagittarius dwarf galaxy is an ongoing merging event at the current epoch (Ibata, Gilmore, & Irwin 1994), and the Magellanic Clouds may ultimately follow the similar fate, as they lose energy via dynamical friction (Tremaine 1976). Signatures of past merging events in the halo were reported by Majewski et al. (1994) in their *in situ* sample of the stars at about 4.5 kpc above the Galactic plane. Helmi & White (1999) argue that the reported clumpiness in the velocity distribution of the halo stars from Majewski et al. is actually

a superposition of two individual streams of stars, possibly arising from a common progenitor.

Clear "fossil evidence" in the solar neighborhood for a previous merger of the Galaxy with what may have been a "Seale & Zinn fragment" has recently been discovered by Helmi et al. (1999, hereafter HWdZZ). These authors examined a subset of the stars in samples from our previous work (BSL; CY), and identified a statistically significant clumping of stars in the angular momentum diagram L_z vs $L_\perp = (L_x^2 + L_y^2)^{1/2}$. The substructure identified by HWdZZ consists of 7 stars (in a sample of 97 stars with [Fe/H] ≤ -1.6 and $D < 1$ kpc), or 12 stars (in a sample of 275 stars with [Fe/H] ≤ -1 and $D < 2.5$ kpc). HWdZZ suggest, based on the observed numbers of stars in this clump, that roughly 10% of the halo stars outside the solar radius may have arisen from a single coherent object with a total mass of about 10^8 $M_\odot$, disrupted during the process of halo formation.

We now consider the HWdZZ result based on our revised catalog. Figure 15 shows the angular momentum diagram of HWdZZ as populated by the stars of our present sample within 2.5 kpc of the Sun. Panels (a) and (b) are for stars in the abundance ranges [Fe/H] ≤ -1.6 and $-1.6 <$ [Fe/H] ≤ -1, respectively. In both of these abundance ranges there exists a clump of stars in the region that HWdZZ pointed out, at $L_\perp \sim 2200$ kpc km s^{-1} and $L_z \sim 1200$ kpc km s^{-1}. In addition to this clump, we identify a possible "trail" (in angular momentum space) which appears to connect the clump and the high L_z region, most clearly evident among the higher abundance stars shown in panel (b). For the purposes of this discussion, we define the "clump" region to be comprised of stars with $2100 < L_\perp < 2600$ kpc km s^{-1} and $800 < L_z < 1500$ kpc km s^{-1} (solid box), and the "trail" region to be comprised of stars having $1250 < L_\perp < 2000$ kpc km s^{-1} and $1200 < L_z < 2000$ kpc km s^{-1} (dotted box), respectively. We include BPS CS 22876-0040 as a "trail" member (triangle in Fig.15a), which is somewhat outside the region defined above, $(L_z, L_\perp) = (1037, 1672)$ kpc km s^{-1}, because this star exhibits similar orbital motions to the "trail" stars examined below.

We note that the angular momentum, $L_\perp$, is not an exact integral of motion in the currently adopted Galactic potential (which consists of a disk and halo component), thus its use may not be generally appropriate for the study of kinematic substructures in the halo. Rather, the so-called third integral, I_3, which is related to $L_\perp$ in a non-spherical potential, should be used. Unfortunately, no general analytic expression exists for I_3. However, the Stäckel form of the currently adopted potential allows one to estimate I_3 in an explicit manner (de Zeeuw 1985; de Zeeuw, Peletier, & Franx 1986; Dejonghe & de Zeeuw 1988), as well as other integrals, such as the orbital energy E and the angular momentum L_z. Expressions for these three integrals are described in the Appendix.

For a spherically symmetric potential, the quantity $(2I_3)^{1/2}$ is equivalent to $L_\perp$. Figure 16 is a plot of $(2I_3)^{1/2}$ vs. L_z (panel a), and $|E|$ vs L_z diagram (panel b), respectively, for the 723 stars from our sample with [Fe/H] ≤ -1 and $D \leq 2.5$ kpc. Filled and open circles denote the stars in the "clump" and "trail" regions of Figure 15, respectively. We note that one star in the "clump"

region of Figure 15 (HD 214161) exhibits quite different orbital parameters than the others (see below), so this star is drawn as a cross in Figure 16. The fact that we see such similar structures in Figures 15 and 16 implies that, along the orbits of the stars constituting the "clump" and "trail", the gravitational potential can be regarded as nearly spherical – the member stars spend the majority of their orbits far from the Galactic plane, where the effect of the disk potential is modest. Also, panel (b) suggests that the orbital energies $|E|$ of the stars in the "clump" are confined to the narrow range near $|E| \simeq 10^5$ km^2 s^{-2}, whereas the stars in the "trail" have a rather diverse range of $|E|$.

Another choice of integrals in the current mass model are the so-called action integrals, **J**. Action integrals are adiabatic invariants, and thus remain unchanged even if the orbital energy E changes via gravitational interaction, provided the time scale for the interaction is sufficiently long compared to the orbital period. One of the actions is J_ϕ, which is equivalent to L_z in an axisymmetric potential. Other suitable actions in the current Stäckel potential, defined in terms of the spheroidal coordinates (λ, ν), are (J_λ, J_ν) (see the Appendix for complete definitions). Panels (c) and (d) of Figure 16 show the distribution of our sample stars in the J_ν vs J_λ and J_ν vs L_z diagrams, respectively. It can been seen that all of the "clump" stars, except for the star HD 214161 ($J_\lambda = 5058, J_\nu = 1223$), exhibit a clear clumpiness in action space, whereas the "trail" stars show a broad distribution in J_ν, but with a rather narrow distribution in J_λ [with the exception of the star CS Ser ($J_\lambda = 6957, J_\nu = 587$)].

From these integrals of motion, we conclude that the "clump" consists of only 9 stars, instead of 12 stars in the HWdZZ result, and the "trail" consists of 9 stars. The kinematic quantities for these stars are listed in Table 6. The orbit of the "clump" is characterized by $Z_{max} \sim 16$ kpc, $r_{ap} \sim 20$ kpc, and $r_{pr} \sim 7$ kpc, which are in good agreement with the HWdZZ result. Note that even though we have tripled the numbers of stars considered in our present sample (728 stars), relative to that of the sample examined by HWdZZ (275 stars), the number of detected clump members has *not* increased. Thus, HWdZZ's conclusion that as much as one-tenth of the halo stars presently located in the solar neighborhood originates from a single object may not apply. We have not considered, as of yet, the impact of the "trail" stars on this argument.

Figure 17 shows the metallicity distribution of the stars in the "clump" (solid histogram) and in the "trail" (dotted histogram) features. The two features seem to share a similar metallicity distribution, though the number of stars involved is still too small for any definite conclusion to be reached. It might be tempting to suggest that the "trail" was formed via the tidal interaction of the precursor object of the "clump" with the Galactic potential, with the "trail" stars gaining some of the orbital angular momentum lost by the precursor object. Such an interaction may have proceeded in a rapid manner, being comparable to the orbital period of the object, so that the actions of the "trail" differ from those of the "clump". Progress on evaluation of this picture will require detailed numerical simulations, which we are presently investigating.

6. Discussion and Conclusion

We have analyzed both the local and global kinematics of 1203 metal-poor stars in the Galaxy with [Fe/H] ≤ -0.6, based on a large, revised, catalog of stars selected without kinematic bias (Paper II). All of these stars have available distance estimates, radial velocities, proper motions, and abundance estimates over the full applicable range in the Milky Way. This is the largest non-kinematically selected sample yet assembled, so the derived kinematic properties are the least affected by systematics as well as statistical fluctuations. We summarize our results below, and discuss them in the context of the formation of the Galaxy.

6.1. Summary of the Results

The local kinematics of the halo population, based on the stars with [Fe/H] ≤ -2.2 and $|Z| < 1$ kpc, are characterized by a radially elongated velocity ellipsoid $(\sigma_U, \sigma_V, \sigma_W) = (141 \pm 11, 106 \pm 9, 94 \pm 8)$ km s^{-1} and a small prograde rotation $< V_\phi >= 30 \sim 50$ km s^{-1} (assuming $V_{LSR} = 220$ km s^{-1}). When additional halo stars at larger $|Z|$ are taken into account, the velocity ellipsoid remains essentially unchanged, but $< V_\phi >$ exhibits a marked decrease (Figs. 2 and 3). We find no evidence for an increase of σ_W at the lowest abundances, as had been previously suggested. At higher metallicities, the stars in our sample exhibit disk-like kinematics, and a higher mean rotation. Specifically, for stars in the abundance interval $-0.7 \leq$ [Fe/H] < -0.6 and with $|Z| < 1$ kpc, we have obtained $(\sigma_U, \sigma_V, \sigma_W) = (46 \pm 4, 50 \pm 4, 35 \pm 3)$ km s^{-1} and $< V_\phi >= 200$ km s^{-1}, which characterize the kinematic parameters of the thick disk. We have also confirmed previous results that there exists a remarkable discontinuity of the rotational properties of the Galaxy at [Fe/H] $\simeq -1.7$ (Fig. 3).

Analysis of a large sample of non-kinematically selected stars provides clear evidence, supporting earlier suspicions based on much smaller samples, that there exists *no correlation between metal abundances and orbital eccentricities* for metal-poor stars of the Milky Way (Fig. 5). Even at the lowest abundances explored in our sample, [Fe/H] ≤ -2.2, about 20% of the stars have $e < 0.4$. In addition, there is a small concentration of high-e stars at [Fe/H] ~ -1.7, which is possibly responsible for the near zero $< V_\phi >$ at the same metallicity. We found that the fraction of the low-eccentricity stars with [Fe/H] ≤ -2.2 remains the same, even as one changes the range of $|Z|$ (Fig. 6a), so such stars belong to the halo, not the MWTD component. On the other hand, stars in intermediate abundance ranges above -2.2 dex exhibit a decrease of low-e stars with increasing $|Z|$, and the fraction of such stars appears to converge at high $|Z|$ to that found for [Fe/H] ≤ -2.2 (Fig. 6b). Both a KS test and a Monte Carlo simulation enable a determination of the structural parameters of the disk component in these abundance ranges. Specifically, the fraction of the disk component is about 30% for $-1.7 <$ [Fe/H] ≤ -1, but is less than 10% for more metal-poor ranges (Fig. 8).

The global kinematics of the halo stars are summarized as follows. In contrast to the claims

of Majewski (1992), and Carney et al. (1996), stars in our sample do *not* show a net retrograde rotation at large Z_{max}, but rather exhibit a near zero systematic rotation (Fig. 10). The difference between our result and that of Carney et al. (1996) probably arises from the (unavoidable) kinematic bias inherent in their sample selection criteria. The observed decrease of $< V_\phi >$ with increasing Z_{max} is continuous, so that it is not possible to conclude that the inner "contracted" population (with a positive $< V_\phi >$) is distinct from an outer "accreted" population, based on the rotational properties of the metal-poor stars alone. Our analysis of the global density distribution of halo stars, based on the reconstruction method developed by SLZ, confirms SLZ's conclusion that the outer halo is quite round (Fig. 12). However, we see no evidence of an overlapping flattened component in addition to the main, nearly spherical one, as was claimed by SLZ. Rather, the density distribution of the halo is better described as nearly spherical in the outer region (beyond $R = 15 - 20$ kpc) and highly flattened in the inner region.

We have confirmed a recent detection of kinematic substructure in the solar neighborhood by HWdZZ, based on a small number of stars which cluster together in the halo angular momentum diagram. We have also found an additional elongated "trail" which appears to connect between HWdZZ's "clump" and the high L_z region (Fig. 14). Further analysis, using several integrals of motion for the "clump," does not result in a dramatic increase in the numbers of stars associated with it, even though the total number of our sample stars is three times as large as that available to HWdZZ.

6.2. Implications for the Formation of the Galaxy

The local and global kinematics of metal-poor stars provide valuable clues for understanding the formation process of the halo and thick disk components in the Galaxy, as well as in disk-type galaxies in general.

If the primordial collapse from the halo to the disk occurred in a monolithic manner, starting from an overdense homogeneous spheroid, one might expect (as predicted by the ELS model) to observe a continuous increase of $< V_\phi >$ for the stars born from the infalling gas, as well as a continuous decrease of their orbital eccentricities with increasing [Fe/H] as the spheroid spins up in order to conserve angular momentum. The fact that we observe no correlation between [Fe/H] and e, and basically no change of $< V_\phi >$ with abundance for stars with [Fe/H] ≤ -1.7 conflicts with this scenario. The lack of an abundance gradient in the halo stars (Carney et al. 1990; CY) is also difficult to interpret in this context. The outer halo, if formed from a monolithic collapse, might be expected to be dominated by radially elongated motions of the stars, but this is actually opposite to the inferred tangentially anisotropic velocity ellipsoid at large distance from the Sun (see Sommer-Larsen et al. 1997). We also note that a small portion of the metal-poor stars having [Fe/H] ~ -1.7 may have been formed from the infalling part of gas, so as to explain both the nearly zero $< V_\phi >$ and the excess number of high-e stars found at [Fe/H] ~ -1.7.

If the halo is assembled from merging and/or accretion of numerous fragments falling into the Galaxy (SZ), one might expect little or no correlation between kinematic and chemical properties, as each fragment has its own chemical history, and the merging process may proceed in a chaotic manner. Our results for the $< V_\phi >$ vs. [Fe/H] and [Fe/H] vs. e relations are basically in agreement with this scenario. The SZ scenario is also consistent with a several Gyr age spread in globular clusters in the outer halo (see, e.g., Rosenberg et al. 1999), and even in field stars (Schuster & Nissen 1989), because the initiation and duration of star formation may not be coherent from fragment to fragment[3]. However, the original SZ scenario seems unlikely to explain our observed vertical gradient of $< V_\phi >$ for halo stars, as well as the highly flattened density distribution of the inner halo, in contrast to the nearly spherical outer halo. Totally incoherent, chaotic merging of SZ fragments would not be expected to produce these "internal" kinematic structures in the halo. It is also unclear as to how the rapidly rotating disk component subsequently formed out of the aftermath of merging (see also Freeman 1996).

SZ first suggested that at least the inner part of the halo may have undergone a coherent contraction in a manner similar to the ELS hypothesis, an idea which has been invoked by subsequent workers to explain the duality of the density, kinematics, and ages of the halo field stars (e.g., SLZ; Norris 1994; Carney et al. 1996; Sommer-Larsen et al. 1997), as well as the age difference between outer and inner globular clusters (Zinn 1996; Rosenberg et al. 1999). This sort of hybrid picture, combining aspects of both the ELS and SZ scenarios, proposes that the outer halo is made up from merging and/or accretion of subgalactic objects, such as dwarf-type satellite galaxies, whereas the inner part of the halo has undergone a dissipative contraction on relatively short timescales. This hybrid model might explain our identification of the inner, flattened, slowly rotating component of the halo with a finite spatial gradient in $< V_\phi >$.

An alternative hypothesis to explain an observed "duality" of the Galactic halo relies on the existence of a thick-disk population of stars even at rather low abundances (MFF; Norris 1994; BSL). If stars with disk-like kinematics have a metallicity distribution which extends below [Fe/H] $= -2$, then a finite fraction of their orbits would be characterized by low e, as found in our present investigation. One possible origin of this MWTD component may be the heating of the pre-existing thin disk triggered by the dissipationless merging of a satellite falling into the disk (Quinn, Hernquist, & Fullagar 1993). Under this hypothesis, the currently observed thin disk, with a vertical scale height of ~ 350 pc, could only have formed *after* the merging event was completed. However, our finding that few thick-disk stars exist with [Fe/H] ≤ -1.7, and no observed increase of σ_W with decreasing [Fe/H], belies the existence of a dynamically hot, proto-disk population at the lowest abundances (see also Norris 1994; Ryan & Lambert 1995; Twarog & Anthony-Twarog 1996). Furthermore, following the results presented in §4.2, we see no evidence for an overlapping

[3]Harris et al. (1997) showed that the most metal-poor globular clusters, such as M92, have essentially the same age everywhere in the halo. As they argued, this result could also be explained within the precepts of the SZ scenario if all of the "SZ fragments" began building the first generation of clusters in the same time period.

flattened component of the halo in addition to a nearly spherical component. An indication that there might exist a significant vertical gradient in $< V_\phi >$ for [Fe/H] ≤ -1.7, compared with a much smaller gradient observed for the thick disk itself, also conflicts with this hypothesis. Thus, we conclude that the formation of the inner flattened halo possibly involves a dissipative contraction, not a dissipationless heating of the proto-disk.

If a hybrid halo formation picture, based on dissipationless merging in the outer halo and dissipative contraction in the inner halo, applies, the question arises as to whether there is a clear boundary distinguishing the two regions. The results presented in §4 suggest no clear distinction between the outer and inner regions of the halo, at least as seen from inspection of the $< V_\phi >$ vs. Z_{max} relation, and the inferred globafl density distribution of the halo. Furthermore, there presently exists no reasonable theoretical explanation for the existence of two distinct populations of stars in the halo. Thus, our current analysis implies that both dissipationless and dissipative processes in the outer and inner halo, respectively, may have occurred more or less in a simultaneous manner.

We now ask whether the above hybrid scenario is a natural consequence of the currently favored theory of galaxy formation based on hierarchical assembly of cold dark matter (CDM) halos (e.g., Peacock 1999). The CDM model postulates that initial density fluctuations in the early Universe have larger amplitudes on smaller scales. Thus, the initially overdense regions that end up forming large galaxies such as our own contain large density fluctuations on subgalactic scales. As a protogalaxy collapses from the general cosmological expansion, these small-scale fluctuations develop into numerous clumps of CDM particles, into which the interstellar gas falls from gravitational attraction. The protogalaxy is thus made up of numerous clumps comprised of a mixture of primordial gas and dark matter, interacting with one another via their mutual gravitational attraction. According to numerical simulations by Steinmetz & Müller (1994; 1995) and Bekki & Chiba (1999), most of the metal-poor stars which presently occupy the outer halo of our Galaxy form in these local, small-scale density fluctuations. Once star formation initiates, the gas inside of these small fragments quickly escapes due to energy feedback from supernovae. Later, these clumps begin to merge with one another, and the aftermath of these essentially dissipationless merging processes exhibits a nearly spherical density distribution with no abundance gradient.

The subsequent evolution of the system may be described in the following way (Bekki & Chiba 1999). As a consequence of the merging of low-mass fragments, a smaller number of more massive clumps develops – within each of these merged clumps one expects to find previously formed metal-poor stars as well as newly born stars. These large clumps continue to accrete gas from their immediate surroundings. These clumps gradually move toward the central region of the system due to both dynamical friction, and dissipative merging with smaller clumps. Then, when the last merging event between the largest clumps occurs, the stars which have been confined inside the clumps are disrupted and spread over the inner part of the halo, whereas a large fraction of the disrupted gas appears to end up in the center of the Galaxy and may form a bulge. As a

consequence, the inner part of the halo should have a flattened density distribution with a finite prograde rotation, as reported here, and its angular momentum distribution may be similar to that of the bulge (Wyse & Gilmore 1992). Also, the stars born from this infalling stage of gas may explain the existence of high-e stars at [Fe/H] ~ -1.7. The simulations conducted to date imply that the thick disk component is partially composed of debris stars, but it is mainly made from diluted gas which has been accreted from the outer part of the halo (Sommer-Larsen et al. 1997). Therefore, although more detailed simulation work is required, CDM models appear to reproduce, at least qualitatively, the overall kinematic properties of the metal-poor stars via both dissipationless merging in the outer halo, and dissipative merging in the inner halo.

It is unknown whether or not evidence for merging events of CDM clumps during the early evolution of the Galaxy might be still preserved as kinematic substructures at the current epoch. Within the currently available precision of space velocities for stars in our sample, typically of the order of 10 to 20 km s^{-1}, the main body of the halo appears to be well mixed in phase space; higher precision measurements of proper motions by the planned astrometric satellites missions (e.g., *FAME, SIM, GAIA*) may be able to disentangle this complex mixture of halo stars (Helmi, Zhao & de Zeeuw 1999). Alternatively, the confirmed kinematic clumping of halo stars presented in §5 may originate from the recent accretion of a satellite galaxy, which has fallen into the Galaxy after the major part of the halo was formed.

Firmer conclusions on the formation of the Galaxy require the assembly and analysis of still larger numbers of stars with accurate distances and proper motions, especially at larger distances from the Sun. Exploration along this line is now in progress. More elaborate numerical modeling of the formation of large spiral galaxies such as the Milky Way is also needed in order to clarify the physical processes that lead to the currently observed dynamics and structure of the halo and disk components. It is of particular importance to model and understand the chemo-dynamical evolution of the system of subgalactic fragments in the course of the Galaxy's collapse. Once a fundamental understanding of the formation and evolution of *our* Galaxy is established, it will then be possible to obtain additional insights into formation of disk-type galaxies in general, by combining our refined picture with the rapidly growing observational database of young galaxies becoming available in the deep realm of the Universe.

We are grateful to the referee, Bruce Carney, for his careful review of the paper and a number of thoughtful suggestions. MC acknowledges partial support from Grants-in-Aid for Scientific Research (09640328) from the Ministry of Education, Science, Sports and Culture of Japan. TCB acknowledges partial support for this work from grant AST 95-29454 from the National Science Foundation.

A. The Stäckel Potential and Integrals of Motion

We briefly describe the properties of the Stäckel potential adopted in this work, and present expressions for the associated integrals of motion. For more details, see, e.g., de Zeeuw (1985), Dejonghe & de Zeeuw (1988), and SLZ.

We define spheroidal coordinates (λ, ϕ, ν), where ϕ corresponds to the azimuthal angle in cylindrical coordinates (R, ϕ, Z), and λ and ν are the roots for τ of

$$\frac{R^2}{\tau + \alpha} + \frac{Z^2}{\tau + \gamma} = 1 \ , \tag{A1}$$

where α and γ are constants, giving $-\gamma \leq \nu \leq -\alpha \leq \lambda$. The coordinate surfaces are spheroids ($\lambda = const.$) and hyperboloids of revolution ($\nu = const.$) with the Z-axis as the rotation axis, where the focal distance $\Lambda = (\gamma - \alpha)^{1/2}$ fixes the coordinate system.

The gravitational potential of the Stäckel type is then written as

$$\varphi(\lambda, \nu) = -\frac{(\lambda + \gamma)G(\lambda) - (\nu + \gamma)G(\nu)}{\lambda - \nu} \ , \tag{A2}$$

where $G(\tau)$ is an arbitrary function. In this work, $G(\tau)$ is the sum of $G_{disk}(\tau)$ from the disk and $G_{halo}(\tau)$ from the massive dark halo. Following SLZ, we adopt the oblate perfect spheroid for $G_{disk}(\tau)$ and the $s = 2$ model of de Zeeuw, Peletier, & Franx (1986) for $G_{halo}(\tau)$.

The Hamiltonian, H, per unit mass, for motion in this potential $\varphi(\lambda, \nu)$ is

$$H = \frac{p_\lambda^2}{2P^2} + \frac{p_\phi^2}{2R^2} + \frac{p_\nu^2}{2Q^2} + \varphi(\lambda, \nu) \ , \tag{A3}$$

where P and Q are the metric coefficients of the spheroidal coordinates, given by

$$P^2 = \frac{\lambda - \nu}{4(\lambda + \alpha)(\lambda + \gamma)}, \ Q^2 = -\frac{\lambda - \nu}{4(\nu + \alpha)(\nu + \gamma)} \ , \tag{A4}$$

and p_λ, p_ϕ, and p_ν are the conjugate momenta to λ, ϕ, and ν, respectively,

$$p_\lambda = P^2 \dot{\lambda} = P v_\lambda, \ p_\phi = R^2 \dot{\phi} = R v_\phi, \ p_\nu = Q^2 \dot{\nu} = Q v_\nu \ . \tag{A5}$$

The velocities v_λ, v_ϕ, and v_ν at a point (λ, ϕ, ν) are the components of the velocity $\mathbf{v}$ along the orthogonal axis defined locally by the spheroidal coordinate system.

The three integrals of motion, $|E|$, I_2, and I_3, are defined as

$$|E| = -H \tag{A6}$$

$$I_2 = \frac{L_z^2}{2} \tag{A7}$$

$$I_3 = \frac{1}{2}(L_x^2 + L_y^2) + \Delta^2 \left[\frac{1}{2} v_z^2 - Z^2 \frac{G(\lambda) - G(\nu)}{\lambda - \nu} \right] \ , \tag{A8}$$

and the action integrals J_λ, J_ϕ, and J_ν are defined as

$$J_\lambda = \frac{1}{2\pi}\oint p_\lambda d\lambda = \frac{2}{\pi}\int_{\lambda_1}^{\lambda_2} p_\lambda d\lambda \tag{A9}$$

$$J_\phi = \frac{1}{2\pi}\oint p_\phi d\phi = L_z \tag{A10}$$

$$J_\nu = \frac{1}{2\pi}\oint p_\nu d\nu = \frac{2}{\pi}\int_{-\gamma}^{\nu_0} p_\nu d\nu \ , \tag{A11}$$

where (λ_1, λ_2) and ν_0 are the turning points of the orbit, defined as the values for which $v_\lambda = 0$ and $v_\nu = 0$, respectively, and $\nu = -\gamma$ defines the equatorial plane. For the evaluation of J_λ, we have taken four times the integrals from λ_1 to λ_2, to maintain symmetry between J_λ and J_ν and ensure continuity of the actions across transitions from one orbital family to another (de Zeeuw 1985).

REFERENCES

Anthony-Twarog, B. J., & Twarog, B. A. 1994, AJ, 107, 1577

Bahcall, J. N., Schmidt, M., & Soneira, R., M. 1982, ApJ, 258, L23

Beers, T. C., & Sommer-Larsen, J. 1995, ApJS, 96, 175 (BSL, Paper I)

Beers, T. C., Chiba, M., Yoshii, Y., Platais, I., Hanson, R. B., Fuchs, B., & Rossi, S. 2000, AJ, submitted (Paper II)

Bekki, K. & Chiba, M. 1999, in the proceedings of the MPA/ESO meeting: the First Stars, ed. A. Weiss (Berlin: Springer-Verlag), in press

Binney, J., & Tremaine, S. 1987, Galactic Dynamics, (Princeton: Princeton University Press)

Bonifacio, P., Centurion, M., & Molaro, P. 1999, MNRAS, 309, 533

Carney, B. W. 1988, in IAU Symp. 126, The Harlow Shapley Symposium on Globular Clusters Systems in Galaxies, eds. J. E. Grindlay & A. G. D. Philip (Dordrecht: Kluwer), p. 133

Carney, B. W. 1999, in The Third Stromlo Symposium: The Galactic Halo, ASP Conference Series, eds. B. K. Gibson, T. S. Axelrod, & M. E. Putman (San Francisco: ASP), p. 230

Carney, B. W. & Latham, D. W. 1986, AJ, 92, 60

Carney, B. W., Latham, D. W., & Laird, J. B. 1988, AJ, 96, 560

Carney, B. W., Latham, D. W., & Laird, J. B. 1990, AJ, 99, 572

Carney, B. W., Aguilar, L, Latham, D. W., & Laird, J. B. 1990, AJ, 99, 201

Carney, B. W., Laird, J. B., Latham, D. W., & Aguilar, L. A. 1996, AJ, 112, 668

Chiba, M., & Yoshii, Y. 1998, AJ, 115, 168 (CY)

Chiba, M., Yoshii, Y., & Beers, T. C. 1999, in The Third Stromlo Symposium: The Galactic Halo, ASP Conference Series, eds. B. K. Gibson, T. S. Axelrod, & M. E. Putman (San Francisco: ASP), p. 273

Dejonghe, H., & de Zeeuw, P. T. 1988, ApJ, 333, 90

de Zeeuw, P. T. 1985, MNRAS, 216, 273

de Zeeuw, P. T., Peletier, R., & Franx, M. 1986, MNRAS, 221, 1001

Dinescu, D. I., Girard, T. M., & van Altena, W. F. 1999, AJ, 117, 1792

Doinidis, S., & Beers, T.C. 1989, ApJ, 340, L57

Eggen, O. J., Lynden-Bell, D., & Sandage, A. R. 1962, ApJ, 136, 748 (ELS)

Freeman, K. C. 1987, ARA&A, 25, 603

Freeman, K. C. 1996, in Formation of the Galactic Halo .... Inside and Out, ASP Conference Series, eds. H. Morrison & A. Sarajedini (San Francisco: ASP), p. 3

Frenk, C., & White, S. D. M. 1980, MNRAS, 193, 295

Harris, W. E. 1976, AJ, 81, 1095

Harris, W. E., Bell, R. A., VandenBerg, D. A., Bolte, M., Stetson, P. B., Hesser, J. E., van den Bergh, S., Bond, H. E., Fahlman, G. G., & Richer, H. B. 1997, AJ, 114, 1030

Hartwick, F. D. A. 1987, in the Galaxy, eds. G. Gilmore & B. Carswell (Cambridge: Cambridge Univ. Press), p. 281

Hawkins, M. R. S. 1984, MNRAS, 206, 433

Helmi, A., & White, S. D. M. 1999, MNRAS, 307, 495

Helmi, A., Zhao, H.S., & de Zeeuw, P.T. 1999, in The Third Stromlo Symposium: The Galactic Halo, ASP Conference Series, eds. B. K. Gibson, T. S. Axelrod, & M. E. Putman (San Francisco: ASP), p. 125

Helmi, A., White, S. D. M., de Zeeuw, P. T., & Zhao, H.S. 1999, Nature, 402, 53

Ibata, R., Gilmore, G. F., & Irwin, M. J. 1994, Nature, 370, 194

Kerr, F. J., & Lynden-Bell, D. 1986, MNRAS, 221, 1023

Kinman, T. D., Suntzeff, N. B., & Kraft, R. P. 1994, AJ, 108, 1722

Larson, R. B. 1974, MNRAS. 166, 585

Larsen, J.A.., & Humphreys, R.M. 1994, ApJ, 436, L149

Layden, A. C. 1995, AJ, 110, 2288

Lee, J.-W., & Carney, B. W. 1999, AJ, 118, 1373

Majewski, S. R. 1992, ApJS, 78, 87

Majewski, S. R., Munn, J. A. & Hawley, S. L. 1994, ApJ, 427, L37

Majewski, S. R., Munn, J. A. & Hawley, S. L. 1996, ApJ, 459, L73

May, A. & Binney, J. 1986, MNRAS, 221, 857

Mihalas, D. & Binney, J. 1981, Galactic Astronomy (San Francisco: Freeman)

Morrison, H. L., Flynn, C., & Freeman, K. C. 1990, AJ, 100, 1191 (MFF)

Norris, J. E. 1986, ApJS, 61, 667

Norris, J. E. 1994, ApJ, 431, 645

Norris, J. E. & Ryan, S. G. 1989, ApJ, 340, 739

Norris, J. E. & Ryan, S. G. 1991, ApJ, 380, 403

Norris, J. E., Bessell, M. S., & Pickles, A. J. 1985, ApJS, 58, 463

Peacock, J. A. 1999, Cosmological Physics (Cambridge: Cambridge University Press)

Preston, G.W., Shectman, S.A., & Beers, T.C. 1991, ApJ, 375, 121

Quinn, P. J., Hernquist, L., & Fullagar, D. P. 1993, ApJ, 403, 74

Ratnatunga, K. U., & Freeman, K. C. 1989, ApJ, 339, 126

Rodgers, A. W., & Paltoglou, G. 1984, ApJ, 283, L5

Rodgers, A. W., & Roberts, W. H. 1993, AJ, 106, 1839

Rosenberg, A., Saviane, I., Piotto, G., & Aparicio, A. 1999, AJ, 118, 2306

Ryan, S. G. 1992, AJ, 104, 1144

Ryan, S. G., & Norris, J. E. 1991, AJ, 101, 1835

Ryan, S. G., & Lambert, D. L. 1995, AJ, 109, 2068

Saha, A. 1985, ApJ, 289, 310

Schuster, W. J. & Nissen, P. E. 1989, A&A, 222, 69

Searle, L. & Zinn, R. 1978, ApJ, 225, 357 (SZ)

Sommer-Larsen, J., & Zhen, C. 1990, MNRAS, 242, 10 (SLZ)

Sommer-Larsen, J., Beers, T. C., Flynn, C., Wilhelm, R., & Christensen, P. R., 1997 ApJ, 481, 775

Steinmetz, M. & Müller, E. 1994, A&A, 281, L97

Steinmetz, M. & Müller, E. 1995, MNRAS, 276, 549

Tremaine, S. D. 1976, ApJ, 203, 72

Twarog, B. A. & Anthony-Twarog, B. J. 1996, AJ, 111, 220

van Albada, T. S. 1982, MNRAS, 201, 939

Wyse, R. F. G. & Gilmore, G. 1992, AJ, 104, 144

Wyse, R. F. G. & Gilmore, G. 1995, AJ, 110, 2771

Yoshii, Y. & Saio, H. 1979, PASJ, 31, 339

Zinn, R. 1985, ApJ, 293, 424

Zinn, R. 1988, in IAU Symp. 126, The Harlow Shapley Symposium on Globular Clusters Systems in Galaxies, ed. J. E. Grindlay & A. G. D. Philip (Dordrecht: Kluwer), 37

Zinn, R. 1996, in Formation of the Galactic Halo .... Inside and Out, ASP Conference Series, eds. H. Morrison & A. Sarajedini (San Francisco: ASP), p. 211

This preprint was prepared with the AAS LaTeX macros v4.0.

TABLE 1A. Mean Velocities and Velocity Dispersions of the Selected Sample

[Fe/H] (dex)	N	$< U >$ (km/s)	$< V >$ (km/s)	$< W >$ (km/s)	σ_U (km/s)	σ_V (km/s)	σ_W (km/s)
			$\|Z\| < 1$ kpc				
-0.6 to -0.8	141	2 ± 4	-30 ± 5	-5 ± 3	50 ± 3	56 ± 3	34 ± 2
-0.8 to -1.0	79	7 ± 10	-62 ± 10	1 ± 6	93 ± 7	86 ± 7	50 ± 4
-1.0 to -1.6	194	8 ± 9	-122 ± 7	-1 ± 6	122 ± 6	104 ± 5	81 ± 4
-1.6 to -2.2	205	23 ± 10	-178 ± 8	-2 ± 6	147 ± 7	115 ± 6	87 ± 4
≤ -2.2	78	17 ± 16	-187 ± 12	-5 ± 11	141 ± 11	106 ± 9	94 ± 8
			$\|Z\| < 4$ kpc				
-0.6 to -0.8	197	4 ± 5	-43 ± 4	-2 ± 3	65 ± 3	62 ± 3	40 ± 2
-0.8 to -1.0	97	2 ± 10	-74 ± 9	3 ± 5	94 ± 7	84 ± 6	49 ± 4
-1.0 to -1.6	280	5 ± 8	-137 ± 6	-4 ± 5	129 ± 5	108 ± 5	81 ± 3
-1.6 to -2.2	327	8 ± 8	-189 ± 7	-1 ± 5	154 ± 6	121 ± 5	86 ± 3
≤ -2.2	141	13 ± 13	-200 ± 10	-5 ± 9	151 ± 9	121 ± 7	103 ± 6

TABLE 1B. Mean Velocities and Velocity Dispersions of the Selected Sample

[Fe/H] (dex)	N	$< U >$ (km/s)	$< V >$ (km/s)	$< W >$ (km/s)	σ_U (km/s)	σ_V (km/s)	σ_W (km/s)
			$\|Z\| < 1$ kpc				
−0.6 to −0.7	85	4 ± 5	-20 ± 5	-3 ± 4	46 ± 4	50 ± 4	35 ± 3
−0.7 to −0.8	56	-1 ± 7	-45 ± 8	-7 ± 4	53 ± 5	61 ± 6	33 ± 3
−0.8 to −1.0	79	7 ± 10	-62 ± 10	1 ± 6	93 ± 7	86 ± 7	50 ± 4
−1.0 to −1.2	56	20 ± 15	-81 ± 12	14 ± 9	109 ± 10	86 ± 8	66 ± 6
−1.2 to −1.4	65	-9 ± 14	-119 ± 13	-3 ± 8	111 ± 10	106 ± 9	65 ± 6
−1.4 to −1.6	73	15 ± 16	-156 ± 12	-12 ± 12	140 ± 12	104 ± 9	102 ± 8
−1.6 to −1.8	84	25 ± 15	-200 ± 14	-9 ± 8	140 ± 11	132 ± 10	72 ± 6
−1.8 to −2.0	65	31 ± 18	-163 ± 13	4 ± 12	142 ± 13	107 ± 9	100 ± 9
−2.0 to −2.3	74	4 ± 19	-161 ± 11	-11 ± 11	161 ± 13	91 ± 8	92 ± 8
−2.3 to −3.0	58	28 ± 18	-196 ± 14	6 ± 12	141 ± 13	109 ± 10	95 ± 9
			$\|Z\| < 4$ kpc				
−0.6 to −0.7	113	8 ± 6	-31 ± 5	-2 ± 4	64 ± 4	55 ± 4	39 ± 3
−0.7 to −0.8	84	-2 ± 7	-59 ± 7	-2 ± 4	67 ± 5	69 ± 5	41 ± 3
−0.8 to −1.0	97	2 ± 10	-74 ± 9	3 ± 5	94 ± 7	84 ± 6	49 ± 4
−1.0 to −1.2	84	10 ± 12	-101 ± 10	8 ± 7	113 ± 9	94 ± 7	68 ± 5
−1.2 to −1.4	89	0 ± 14	-136 ± 11	-4 ± 8	133 ± 10	105 ± 8	74 ± 6
−1.4 to −1.6	107	4 ± 13	-167 ± 11	-14 ± 9	138 ± 10	113 ± 8	94 ± 6
−1.6 to −1.8	127	14 ± 13	-198 ± 11	-4 ± 7	148 ± 9	124 ± 8	80 ± 5
−1.8 to −2.0	104	17 ± 15	-181 ± 12	-7 ± 9	149 ± 10	119 ± 8	93 ± 6
−2.0 to −2.3	129	-19 ± 14	-191 ± 11	7 ± 8	162 ± 10	121 ± 8	91 ± 6
−2.3 to −3.0	101	35 ± 14	-198 ± 12	-5 ± 10	139 ± 10	123 ± 9	104 ± 7

TABLE 2. Rotational Properties of the Selected Sample

[Fe/H] range (dex)	N^a	$< V_\phi >$ (km/s)	σ_ϕ (km/s)	$< V_\phi > / \sigma_\phi$	$< V_\phi >_{pm}^{FW\,b}$ (km/s)	N^c	$< V_\phi >_{all}^{FW\,d}$ (km/s)
			$\|Z\| < 1$ kpc				
-0.6 to -0.7	85	201 ± 5	50 ± 4	3.98 ± 0.33	211 ± 5	106	210 ± 5
-0.7 to -0.8	56	175 ± 8	61 ± 6	2.88 ± 0.31	185 ± 10	68	187 ± 9
-0.8 to -1.0	79	161 ± 10	85 ± 7	1.90 ± 0.19	164 ± 15	105	167 ± 14
-1.0 to -1.2	56	138 ± 12	86 ± 8	1.60 ± 0.20	109 ± 21	82	122 ± 17
-1.2 to -1.4	65	100 ± 13	107 ± 9	0.94 ± 0.15	80 ± 25	95	88 ± 20
-1.4 to -1.6	73	65 ± 12	104 ± 9	0.63 ± 0.13	4 ± 24	102	-2 ± 22
-1.6 to -1.8	84	21 ± 14	132 ± 10	0.16 ± 0.11	5 ± 22	124	22 ± 18
-1.8 to -2.0	65	58 ± 13	106 ± 9	0.55 ± 0.13	54 ± 29	110	29 ± 27
-2.0 to -2.3	74	59 ± 11	91 ± 8	0.65 ± 0.13	33 ± 40	133	37 ± 26
-2.3 to -3.0	58	25 ± 14	106 ± 10	0.23 ± 0.13	33 ± 36	95	76 ± 29
			$\|Z\| < 1.6$ kpc				
-0.6 to -0.7	101	195 ± 5	52 ± 4	3.76 ± 0.28	211 ± 6	133	208 ± 5
-0.7 to -0.8	68	174 ± 7	59 ± 5	2.96 ± 0.28	186 ± 9	89	181 ± 9
-0.8 to -1.0	88	155 ± 9	85 ± 6	1.82 ± 0.17	163 ± 15	125	169 ± 13
-1.0 to -1.2	75	129 ± 10	85 ± 7	1.52 ± 0.17	113 ± 19	112	121 ± 14
-1.2 to -1.4	77	94 ± 12	105 ± 8	0.89 ± 0.14	75 ± 23	114	89 ± 18
-1.4 to -1.6	93	60 ± 11	106 ± 8	0.57 ± 0.11	3 ± 22	132	-3 ± 19
-1.6 to -1.8	119	21 ± 11	125 ± 8	0.17 ± 0.09	-1 ± 20	178	17 ± 16
-1.8 to -2.0	85	48 ± 12	109 ± 8	0.44 ± 0.11	48 ± 25	153	37 ± 23
-2.0 to -2.3	108	37 ± 12	123 ± 8	0.30 ± 0.10	11 ± 33	194	27 ± 21
-2.3 to -3.0	84	28 ± 13	116 ± 9	0.24 ± 0.11	15 ± 33	146	54 ± 25
			$\|Z\| < 4$ kpc				
-0.6 to -0.7	113	189 ± 5	55 ± 4	3.45 ± 0.25	211 ± 6	150	208 ± 5
-0.7 to -0.8	84	162 ± 8	69 ± 5	2.35 ± 0.21	185 ± 9	111	179 ± 9
-0.8 to -1.0	97	149 ± 8	84 ± 6	1.78 ± 0.16	162 ± 14	147	168 ± 12
-1.0 to -1.2	84	119 ± 10	94 ± 7	1.27 ± 0.15	115 ± 18	126	117 ± 14
-1.2 to -1.4	89	83 ± 11	106 ± 8	0.78 ± 0.12	61 ± 22	130	79 ± 17
-1.4 to -1.6	107	53 ± 11	112 ± 8	0.48 ± 0.10	8 ± 20	150	0 ± 18
-1.6 to -1.8	127	23 ± 11	123 ± 8	0.19 ± 0.09	-1 ± 19	188	15 ± 16
-1.8 to -2.0	104	40 ± 11	113 ± 8	0.35 ± 0.10	39 ± 22	181	24 ± 20
-2.0 to -2.3	129	26 ± 11	122 ± 8	0.22 ± 0.09	22 ± 31	221	35 ± 20
-2.3 to -3.0	101	23 ± 12	121 ± 9	0.19 ± 0.10	13 ± 32	178	43 ± 23

[a]Number of stars with available proper motions.

[b]Based on the FW method for stars with available proper motions.

[c]Number of stars with available radial velocities.

[d]Based on the FW method for stars with available radial velocities.

TABLE 3. Dependence of Rotation Velocity on $|Z|$ for the Selected Sample

$<\|Z\|>$ (kpc)	N	$<V_\phi>$ (km/s)	σ_ϕ (km/s)	$<V_\phi>/\sigma_\phi$
		$-2.4 \leq$[Fe/H]≤ -1.9		
0.27	50	73 ± 14	98 ± 10	0.74 ± 0.16
0.47	50	56 ± 14	97 ± 10	0.58 ± 0.15
0.62	50	50 ± 14	100 ± 10	0.50 ± 0.15
0.74	50	38 ± 14	101 ± 10	0.37 ± 0.15
0.88	50	32 ± 13	94 ± 10	0.34 ± 0.15
1.04	50	19 ± 16	112 ± 11	0.17 ± 0.14
1.24	50	0 ± 21	147 ± 15	0.00 ± 0.14
1.49	50	3 ± 20	142 ± 14	0.02 ± 0.14
1.87	50	-8 ± 20	143 ± 14	-0.05 ± 0.14
		$-0.8 \leq$[Fe/H]≤ -0.6		
0.01	50	203 ± 5	34 ± 3	6.01 ± 0.62
0.02	50	200 ± 6	42 ± 4	4.74 ± 0.50
0.09	50	190 ± 7	52 ± 5	3.68 ± 0.40
0.24	50	185 ± 8	57 ± 6	3.27 ± 0.36
0.46	50	177 ± 10	72 ± 7	2.47 ± 0.29
0.71	50	179 ± 10	70 ± 7	2.56 ± 0.29
1.01	50	171 ± 9	64 ± 6	2.68 ± 0.31
1.75	64	143 ± 8	68 ± 6	2.12 ± 0.23

TABLE 4. Parameters of the MWTD at $|Z| < 1$ kpc[a]

[Fe/H] (dex)	<[Fe/H]> (dex)	N	$\sigma_{\phi,disk}$ (km/s)	F
-0.6 to -1.0	-0.76	220	40	0.85
-1.0 to -1.7	-1.37	234	47	0.29
-1.7 to -2.2	-1.93	165	41	0.08
≤ -2.2	-2.48	78	16	0.05

[a]On the assumption that $<V_\phi>_{halo} = 33$ km s^{-1} and $\sigma_{\phi,halo} = 106$ km s^{-1} for the halo and $<V_\phi>_{disk} = 200$ km s^{-1} for the disk.

TABLE 5. List of Likely Metal-Weak Thick Disk Stars

Star	RA (2000.0)	DEC	Type	[Fe/H] (dex)	Z (kpc)	V_R (km/s)	V_ϕ (km/s)	V_Z (km/s)
BPS CS 29503-0031	00 13 54.85	−27 36 38.8	TO	−2.09	−0.68	7	158	−32
CD-23 72	00 16 16.54	−22 34 40.6	G	−1.17	−0.18	−9	210	−17
BPS CS 30339-0076	00 37 21.77	−35 53 57.0	SG	−2.18	−0.79	−26	188	−29
BD-20 170	00 57 10.21	−19 49 58.2	G	−1.31	−0.40	24	198	12
HD 13359	02 10 07.03	−20 45 51.5	G	−1.66	−0.32	−17	215	−26
HD 15395	02 26 44.72	−54 32 33.9	TO	−1.14	−0.07	−34	172	−2
HD 17072	02 40 39.99	−69 13 58.7	AGB	−1.00	−0.09	−6	161	−17
HD 18710	02 58 42.59	−48 43 56.6	G	−1.05	−0.56	13	283	−2
BPS CS 22182-0021	04 18 14.53	−31 29 52.6	TO	−1.26	−0.68	18	222	9
HD 33073	05 06 32.00	−28 33 36.9	G	−1.30	−0.11	24	164	−21
HD 33605	05 12 34.10	+27 36 15.4	G	−1.51	−0.09	18	248	16
HD 241894	05 15 16.14	+29 17 02.9	G	−1.22	−0.06	23	241	22
HD 36054	05 30 03.22	+23 45 31.5	G	−1.38	−0.03	−6	224	5
HD 36931	05 36 26.16	+30 35 26.2	G	−2.09	−0.01	−6	231	−4
HD 246370	05 41 52.89	+26 02 22.5	G	−1.92	−0.02	0	235	11
HD 251432	06 06 01.65	+25 16 57.8	G	−1.05	0.03	−18	226	7
HD 251549	06 06 34.95	+26 19 45.2	G	−2.08	0.06	8	256	−15
HD 252041	06 08 23.76	+28 58 36.2	G	−1.76	0.05	−31	218	−4
HD 41994	06 09 26.56	+27 11 38.0	G	−1.57	0.03	1	224	3
HD 252370	06 09 38.43	+28 21 38.3	G	−1.37	0.05	−33	216	−10
V* SZ Lyn	08 09 35.76	+44 28 17.8	V	−1.16	0.31	42	166	−5
HD 77941	09 04 01.40	−42 53 31.3	G	−1.03	0.03	−11	164	2
HD 103295	11 53 37.06	−28 38 13.1	G	−1.04	0.12	43	221	3
BD+30 2282	12 29 33.92	+30 04 51.4	G	−1.12	0.90	9	286	3
HD 108976	12 31 03.11	+27 43 49.3	G	−1.43	0.08	−6	227	5
MA 30 210	12 31 36.36	+30 12 53.2	G	−1.04	0.52	24	170	5
Basel SA 57-1016	13 08 18.09	+29 27 39.6	D	−1.04	0.58	7	208	−3
HD 120559	13 51 40.79	−57 26 04.7	D	−1.13	0.00	20	185	−30
HD 128188	14 35 46.83	−11 24 12.2	G	−1.37	0.51	21	196	−26
V* AV Ser	16 01 20.75	+00 44 25.1	RRV	−1.20	0.72	34	281	−34
V* ST Oph	17 33 59.38	−01 04 51.6	RRV	−1.30	0.42	−5	221	25
V* V494 Sco	17 40 47.36	−31 32 43.3	RRV	−1.01	−0.01	−36	229	9
V* AC Her	18 30 16.24	+21 52 00.6	V	−1.20	0.22	11	227	22
HD 171496	18 36 07.50	−24 26 11.3	G	−1.12	−0.05	32	218	34
HD 199854	21 00 13.65	−15 06 52.0	FHB	−1.94	−0.27	−26	239	17
BD+46 3330	21 28 48.98	+47 06 54.5	G	−1.93	−0.03	6	223	3
BPS CS 29495-0071	21 47 37.68	−26 09 36.9	TO	−1.86	−0.38	15	182	30
BD+43 4063	21 50 40.42	+43 50 42.7	G	−1.05	−0.02	−9	250	1
BD+47 3617	21 57 02.84	+48 22 49.9	G	−1.76	−0.02	−13	211	6
BD+46 3563	22 04 15.27	+47 24 16.6	G	−1.75	−0.03	−1	232	2
HD 211744	22 20 09.93	−44 21 52.6	G	−1.03	−0.15	22	194	−13
BPS CS 29512-0076	22 27 43.06	−11 21 24.2	TO	−1.97	−0.69	−17	238	29
HD 213487	22 32 03.30	−21 35 56.6	G	−1.25	−0.41	−1	220	−3
BPS CS 30493-0071	23 16 30.78	−35 34 35.8	TO	−2.20	−0.63	39	185	−10
BPS CS 30493-0072	23 17 05.16	−36 21 56.9	TO	−1.77	−0.90	−14	209	−13
V* AC And	23 18 02.35	+48 46 58.4	V	−1.16	−0.22	−15	190	5

TABLE 6. Stars in the Kinematic Substructures[a]

Star	[Fe/H] (dex)	L_z (kpc km/s)	$\sqrt{2I_3}$ (kpc km/s)	$\|E\|$ (km^2/s^2)	J_λ (kpc km/s)	J_ν (kpc km/s)	Z_{max} (kpc)	r_{pr} (kpc)	r_{ap} (kpc)
				Clump					
BPS CS 29504−0044	−2.04	1076	2462	108369	603	1218	15.2	7.3	17.7
CD−36 1052	−2.19	1200	2540	104220	781	1232	16.6	7.5	19.7
V* TT Lyn	−1.56	854	2466	109130	679	1326	15.9	6.7	17.7
BD+10 2495	−1.83	1459	2548	100149	963	1134	17.3	7.8	21.7
HD 119516	−2.49	1345	2425	102127	1018	1065	16.8	7.1	21.1
BD+30 2611	−1.32	1301	2627	102448	758	1271	17.0	8.0	20.3
HD 175305	−1.45	1293	2692	101214	798	1334	17.7	8.2	20.8
V* XZ Cyg	−1.44	1231	2497	109357	358	1190	13.8	8.4	16.5
BPS CS 29513−0031	−2.79	1304	2671	99596	980	1305	18.5	7.8	22.0
				Trail					
BPS CS 22876−0040	−2.20	1037	2011	118146	480	816	11.3	5.9	14.4
V* CS Eri	−1.41	1438	2138	109407	635	802	12.6	7.1	17.5
V* U Cae	−1.11	1588	1464	125704	25	327	5.1	8.2	10.1
BD+29 2356	−1.06	1266	1816	125205	41	606	7.2	7.8	10.4
V* RX CVn	−1.31	1866	1673	113966	308	410	7.7	8.0	14.9
HD 128279	−2.20	1326	2174	116332	149	875	10.2	8.4	13.4
V* WY Dra	−1.66	1296	1480	128103	205	366	6.0	6.0	11.0
V* YZ Aqr	−1.55	1596	1960	111924	477	633	10.5	7.4	16.2
BPS CS 29513−0032	−2.02	1551	1657	104686	1445	427	11.4	5.3	21.1

[a]Based on the Galactic potential utilized in §3.

Fig. 1.— Distribution of the velocity components (U, V, W) vs. [Fe/H] for the 1203 stars with available proper motions.

Fig. 6.— (a) The relation between [Fe/H] and e for 1203 stars with [Fe/H] ≤ -0.6. Note the diverse range of e even at low metallicities. (b) The relation between [Fe/H] and mean eccentricities $< e >$ (solid line with filled circles), calculated by passing a box of width $N = 100$ stars (ordered by metallicity), with an overlap of 20 stars each. The dashed line denotes the result of Carney et al. (1996) for their high-proper-motion sample.

Fig. 11.— The relation between V_ϕ and Z_{max} for stars with [Fe/H] ≤ -1.5. (a) For the sample analyzed by Carney et al. (1996). Filled circles denote their original data, whereas crosses denote our re-calibration of the same data using the currently adopted Galactic potential. (b) For the simulated, kinematically biased sample via a Monte Carlo method, to reproduce the Carney et al. result. The lower limit to the measured proper motions is set to 0.26" yr^{-1}. (c) For the present sample. In all panels, solid lines with error bars show local regression lines through the data. Note that the non-kinematically selected stars in (c) show no net rotation at large Z_{max}, in contrast to the Carney et al. sample (a).

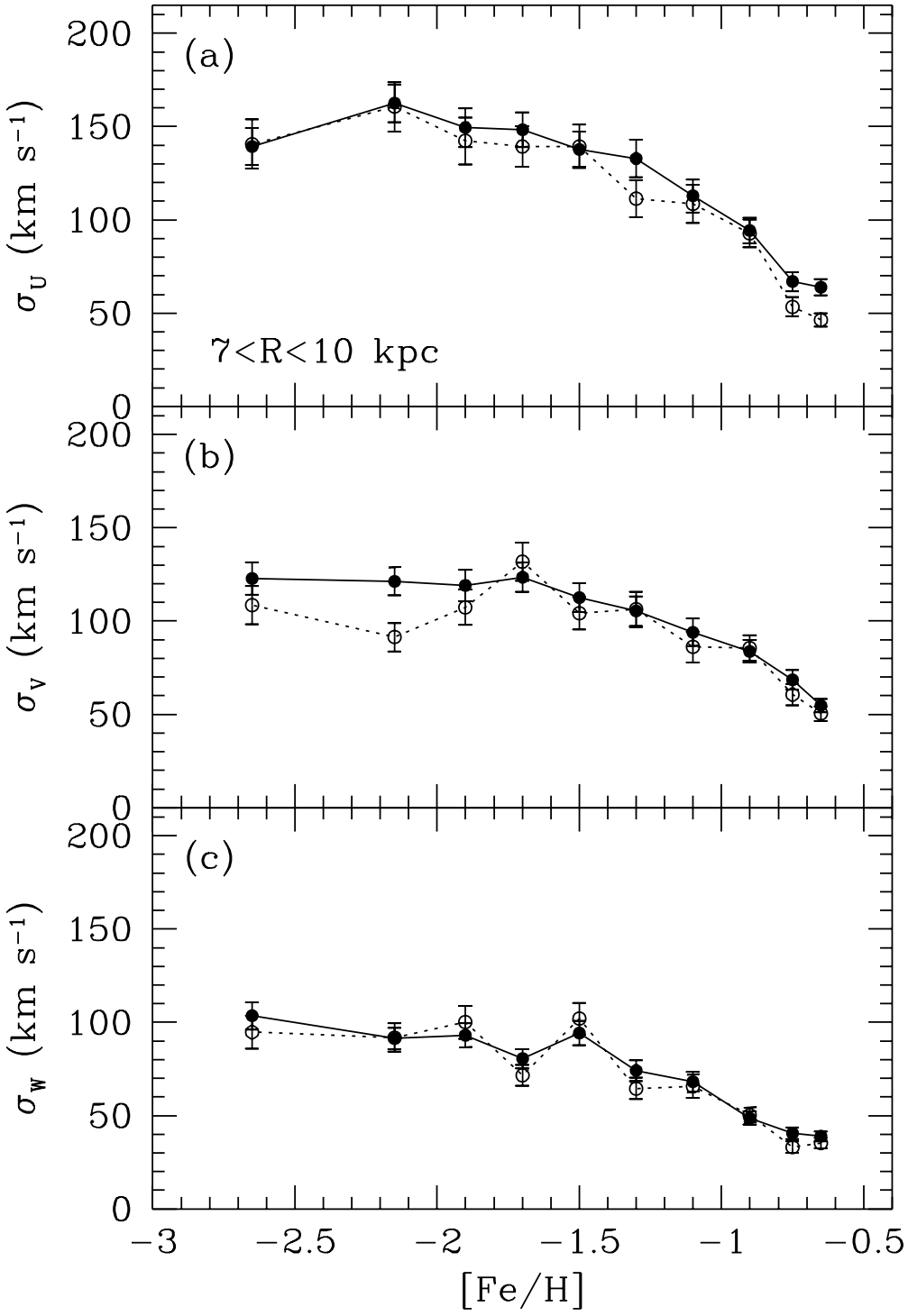

Fig. 2.— Distribution of the velocity dispersions ($\sigma_U, \sigma_V, \sigma_W$) vs. [Fe/H] for the Selected Sample with $7 < R < 10$ kpc, $D < 4$ kpc, and $V_{RF} \leq 550$ km s^{-1}. Filled and open circles denote the stars at $|Z| < 1$ kpc and $|Z| < 4$ kpc, respectively.

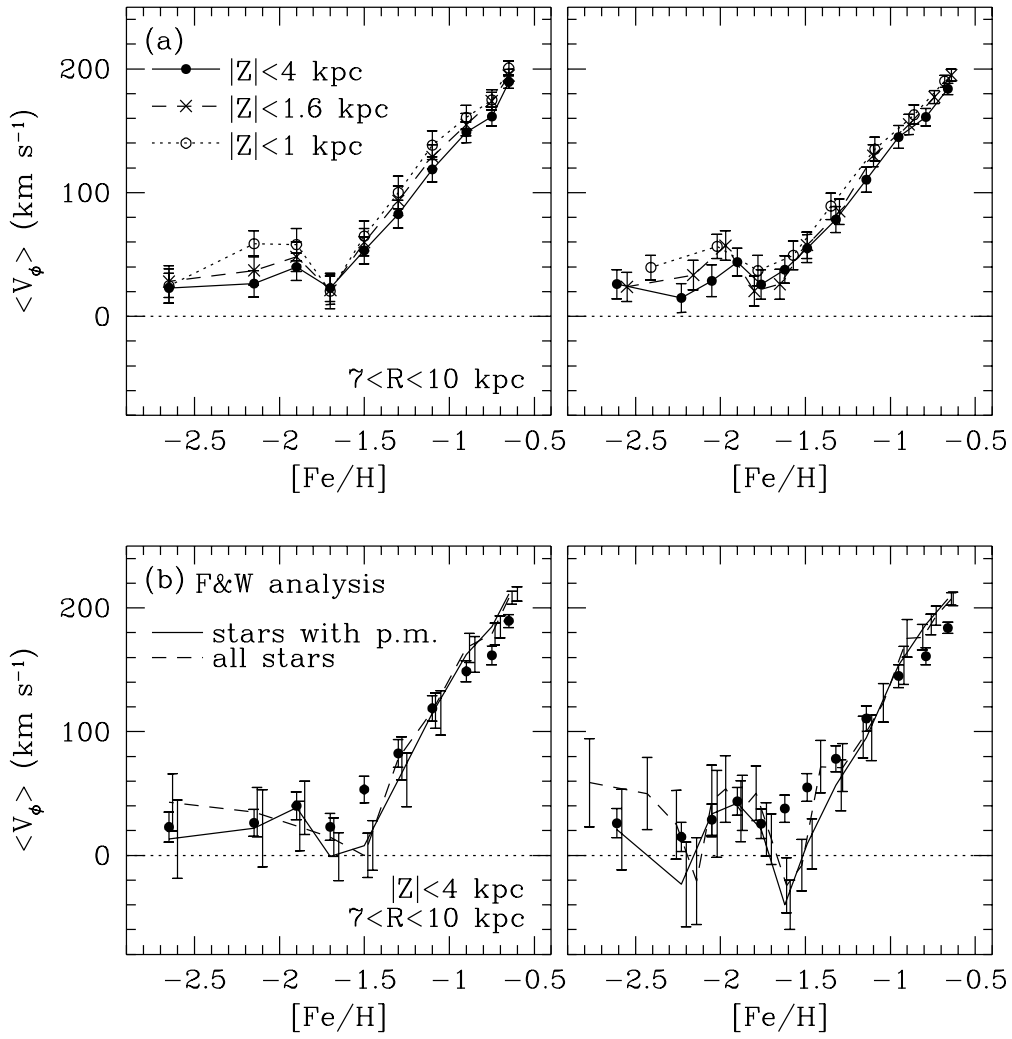

Fig. 3.— Distribution of the mean rotational velocities $< V_\phi >$ vs. [Fe/H] for the Selected Sample, assuming an LSR rotation velocity of 220 km s^{-1}. Left-hand panels show the results for characteristic abundance ranges, whereas in the right-hand panels, we calculate $< V_\phi >$ by passing a box of width $N = 100$ stars (ordered by metallicity), with an overlap of 20 stars each. (a) Based on the full knowledge of proper motions and radial velocities. Filled circles, crosses, and open circles correspond to the stars at $|Z| < 4$ kpc, $|Z| < 1.6$ kpc, and $|Z| < 1$ kpc, respectively. (b) Based on the Frenk & White methodology using radial velocities alone. The solid line denotes $< V_\phi >$ for the stars with available proper motions at $|Z| < 4$ kpc, i.e. the same sample as in panel (a). The dashed line denotes $< V_\phi >$ for the stars with available radial velocities and $|Z| < 4$ kpc. For comparison, we plot the filled circles from panel (a).

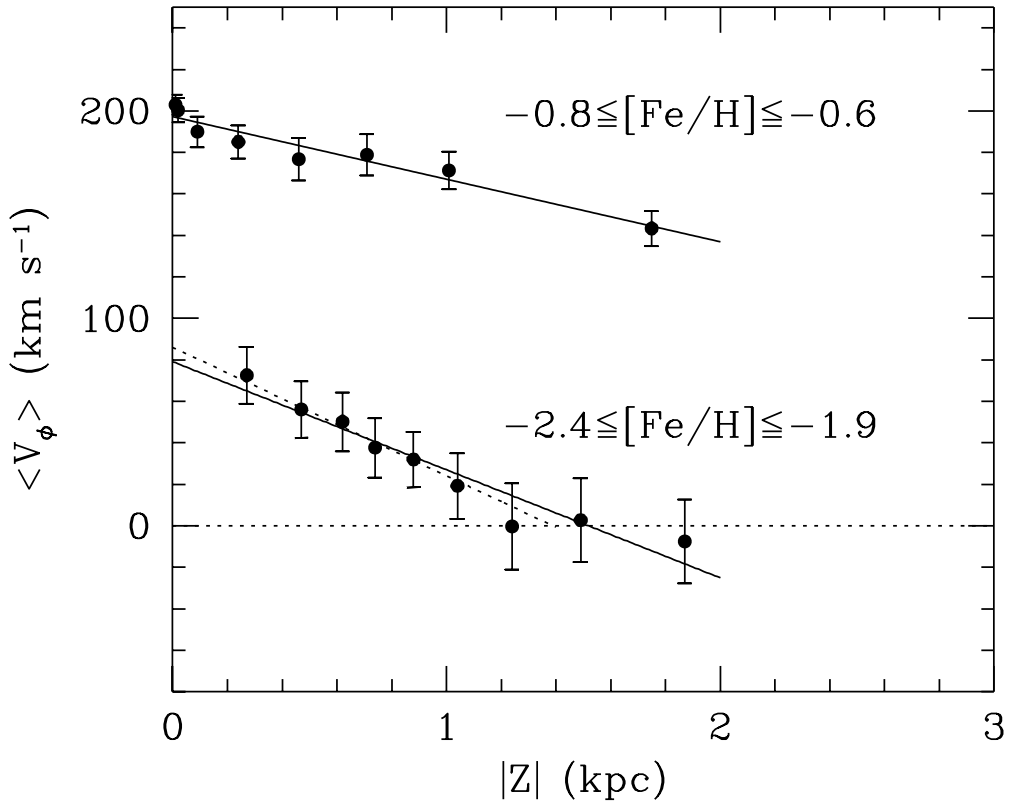

Fig. 4.— Distribution of the mean rotational velocities $< V_\phi >$ vs. $|Z|$ for stars of the Selected Sample, in the abundance ranges $-2.4 \leq$ [Fe/H] ≤ -1.9 and $-0.8 \leq$ [Fe/H] ≤ -0.6, respectively. The binning in $|Z|$ is made by sweeping a box of 50 stars through the data (ordered by $|Z|$), with an overlap of 30 stars. Solid lines are least-square fits to the data. The dotted line for $-2.4 \leq$ [Fe/H] ≤ -1.9 is the fit obtained after excluding the last point at $|Z| = 1.76$ kpc.

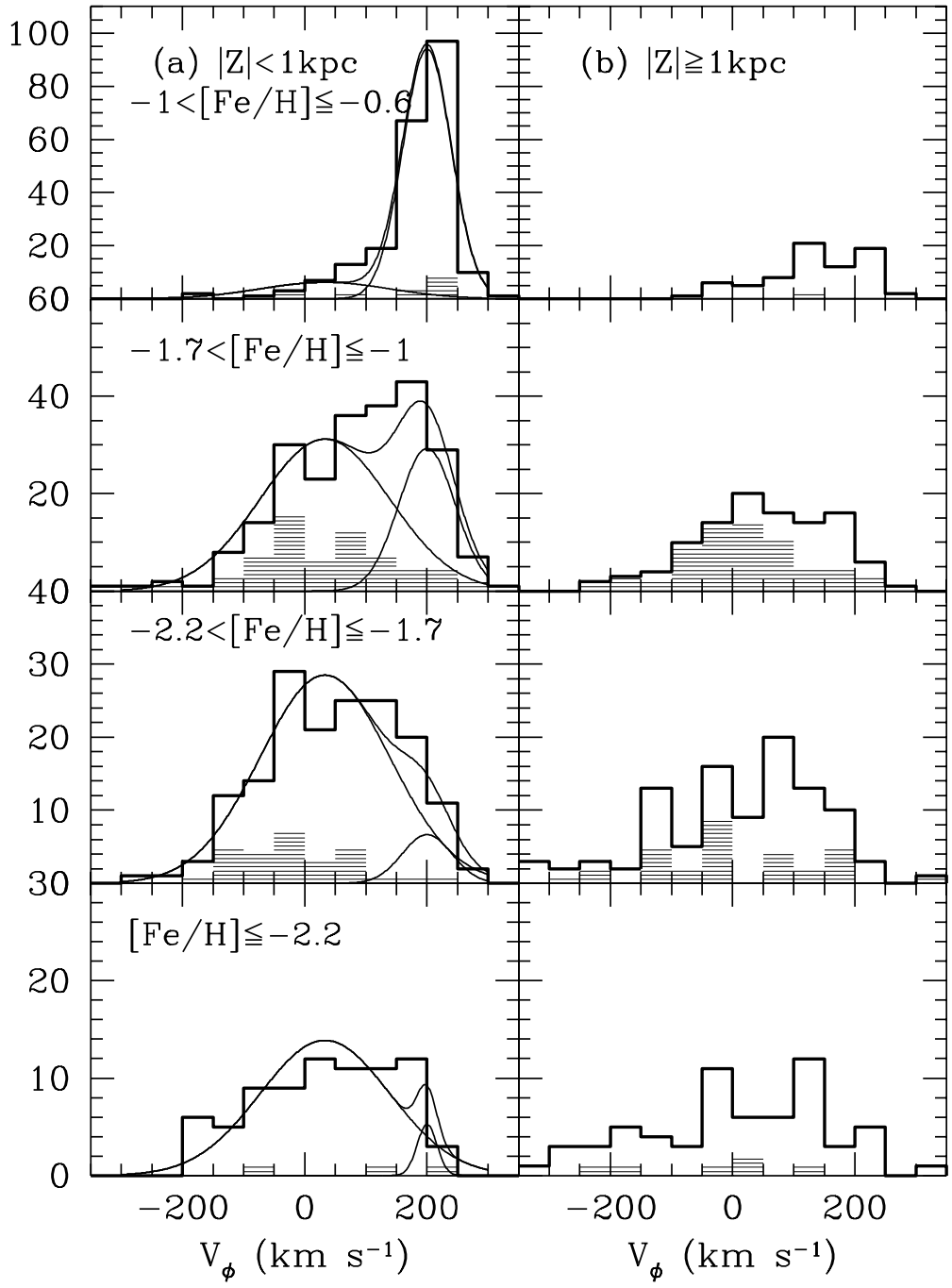

Fig. 5.— Distribution of V_ϕ in different metallicity ranges for the stars with available proper motions. Solid and shaded histograms denote all stars and RR Lyrae stars, respectively, for (a) $|Z| < 1$ kpc and (b) $|Z| \geq 1$ kpc. Also shown in the left-hand panels are the results of the maximum likelihood analysis for reproducing the V_ϕ distribution at $|Z| < 1$ kpc, based on a mixture of two Gaussian components, which we associate with the halo and thick disk.

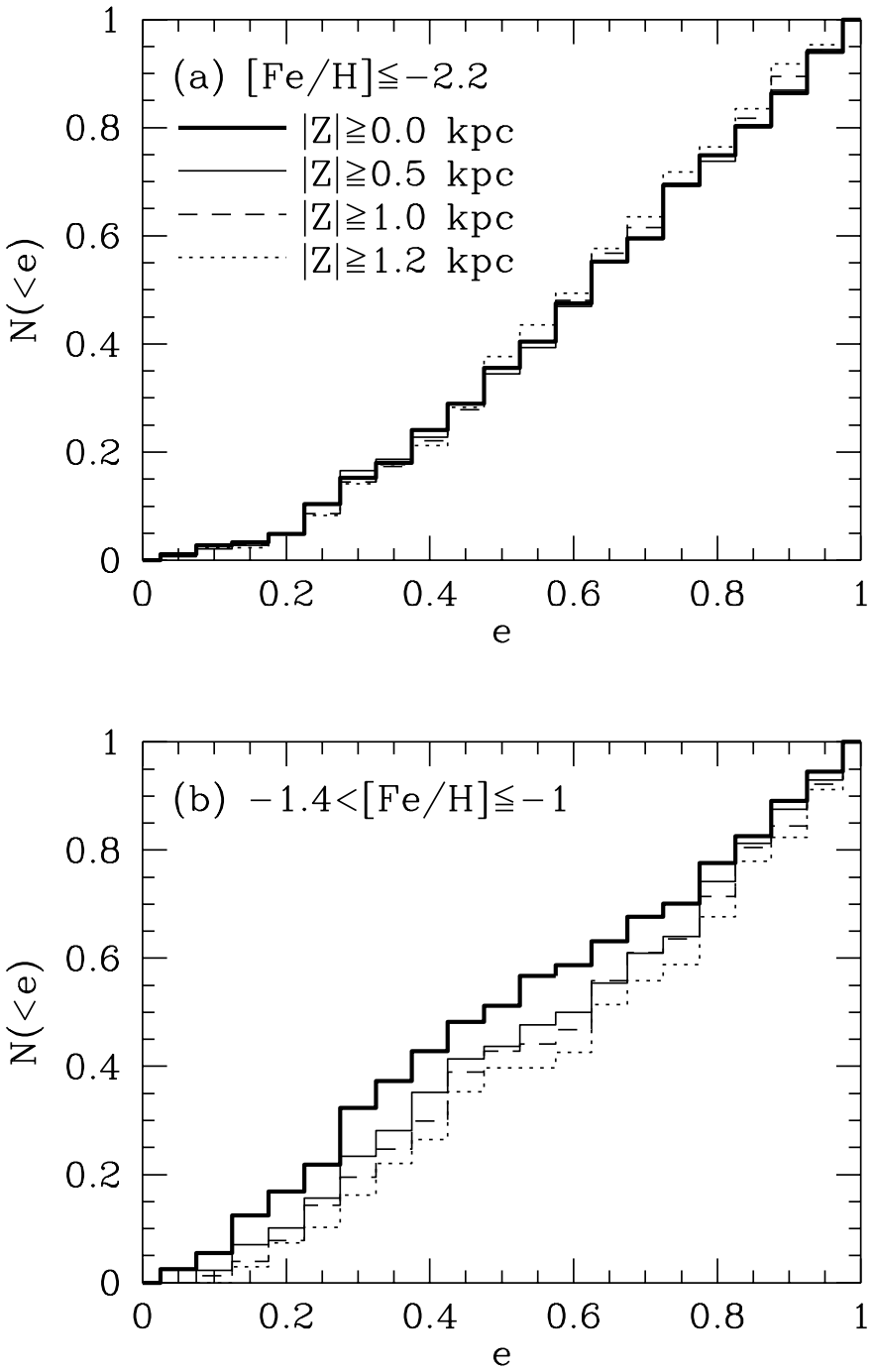

Fig. 7.— Cumulative e distributions, $N(< e)$, in the two abundance ranges (a) [Fe/H] ≤ -2.2, and (b) $-1.4 <$[Fe/H] ≤ -1. The thick solid, thin solid, dashed, and dotted histograms denote the stars at $|Z| \geq 0.0$ kpc (all stars), $|Z| \geq 0.5$ kpc, $|Z| \geq 1.0$ kpc, and $|Z| \geq 1.2$ kpc, respectively.

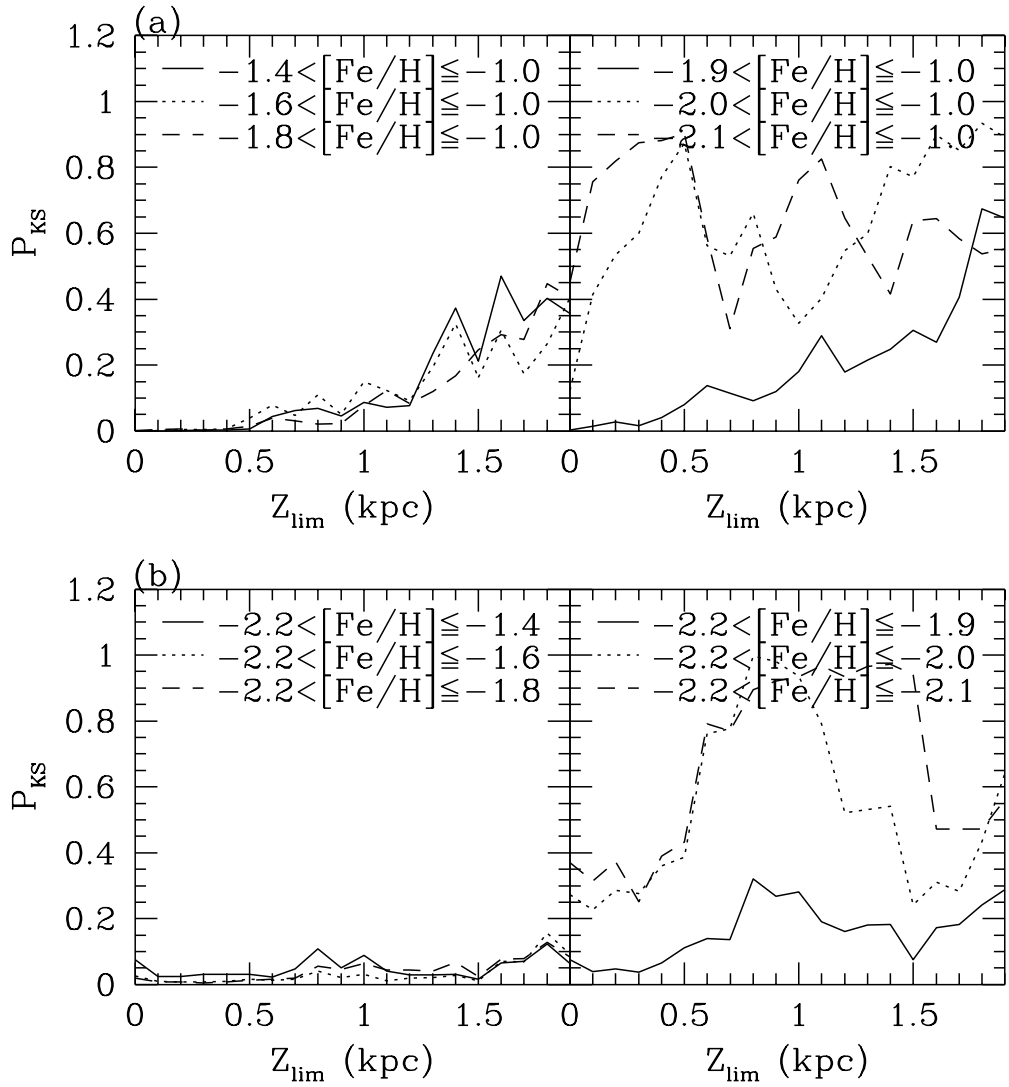

Fig. 8.— (a) Kolmogorov-Smirnoff probabilities for the stars included in each abundance range at $|Z| > Z_{lim}$, for evaluation of the null hypothesis that the differential e distribution, $n(e)$, is drawn from the same parent population as the "pure" halo with [Fe/H] ≤ -2.2 and $|Z| < 1$ kpc. The lines denote results obtained when the lower limit of each abundance range is varied, while the upper limit is fixed at [Fe/H] $= -1$. (b) Same as in (a), but for the more metal-poor range. The lines denote results obtained when the upper limit of each abundance range is varied, while the lower limit is fixed at [Fe/H] $= -2.2$.

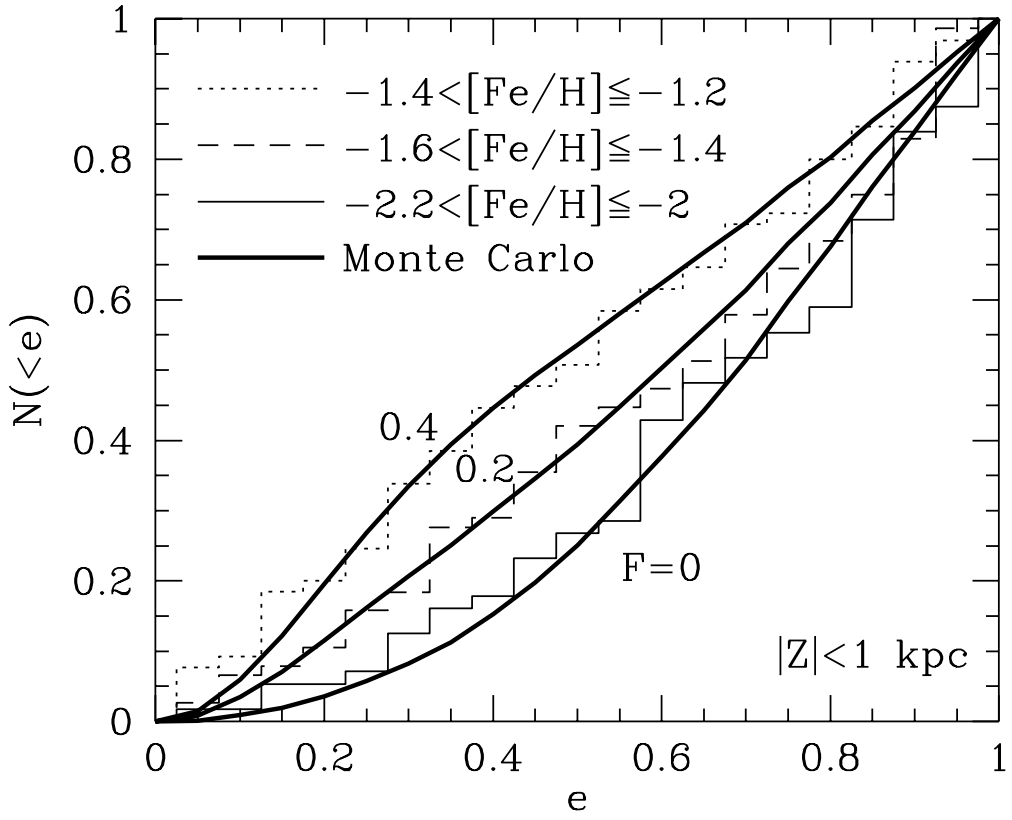

Fig. 9.— Comparisons of observed $N(< e)$ in the solar neighborhood in various abundance ranges with Monte Carlo results, based on a mixture of two Gaussian components, taken to represent the halo and thick disk, where the disk fraction is denoted as F. We take $< V_\phi >= +33$ km s^{-1} and $(\sigma_U, \sigma_V, \sigma_W) = (141, 106, 94)$ km s^{-1} for the halo, and $< V_\phi >= +200$ km s^{-1} and $(\sigma_U, \sigma_V, \sigma_W) = (46, 50, 35)$ km s^{-1} for the thick disk.

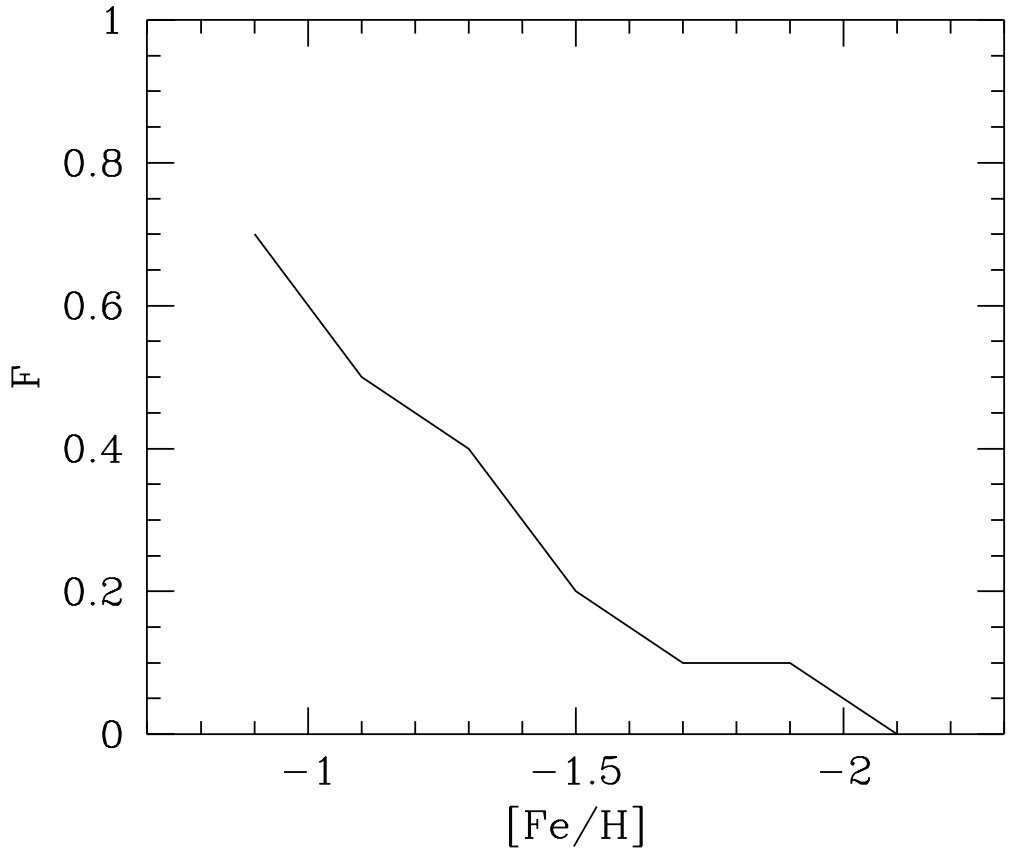

Fig. 10.— The fraction F of the thick disk at $|Z| < 1$ kpc as a function of [Fe/H], derived by the comparison between the observed and predicted $N(< e)$.

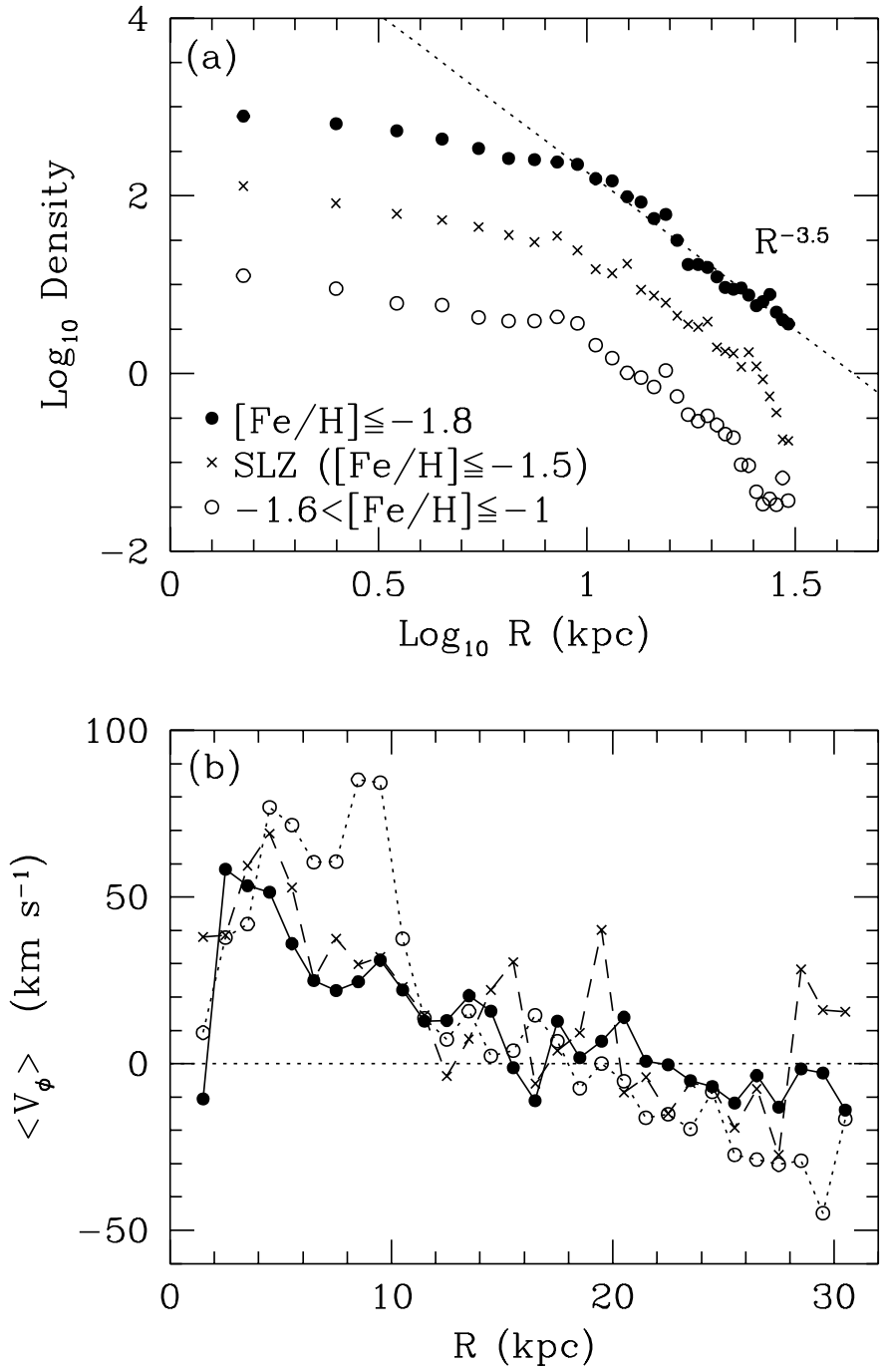

Fig. 12.— (a) Density distributions of the reconstructed halo in the Galactic plane, for [Fe/H] ≤ -1.8 (filled circles) and $-1.6 <$ [Fe/H] ≤ -1 (open circles). Both plots have been shifted arbitrarily along the vertical axis. The dotted line denotes the power-law model with exponent $\beta = -3.5$. For comparison, the density distribution based on the SLZ sample with [Fe/H] ≤ -1.5 is shown as crosses. (b) Mean rotational velocities of the reconstructed halo projected onto the Galactic plane. Symbols are the same as in (a).

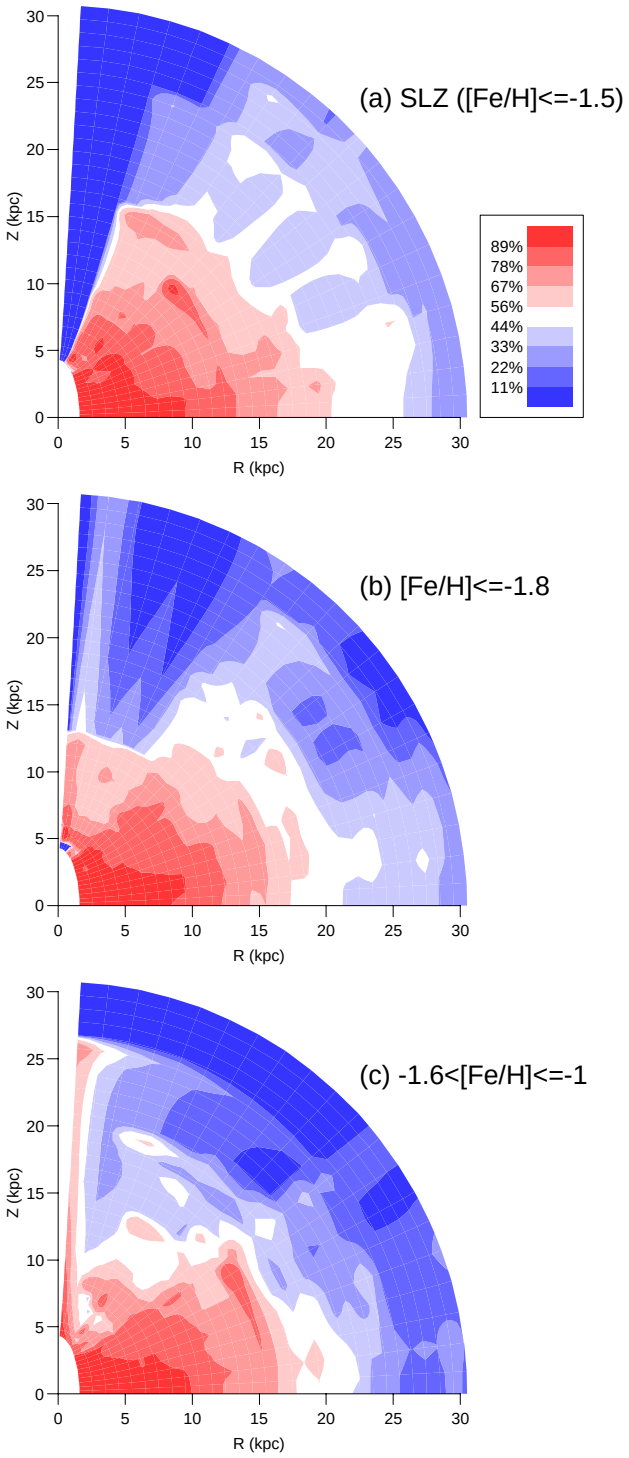

Fig. 13.— Equidensity contours for the reconstructed halo in the (R, Z) plane. (a) For the SLZ sample with [Fe/H] ≤ -1.5, (b) for our sample with [Fe/H] ≤ -1.8, and (c) for our sample with $-1.6 <$ [Fe/H] ≤ -1.

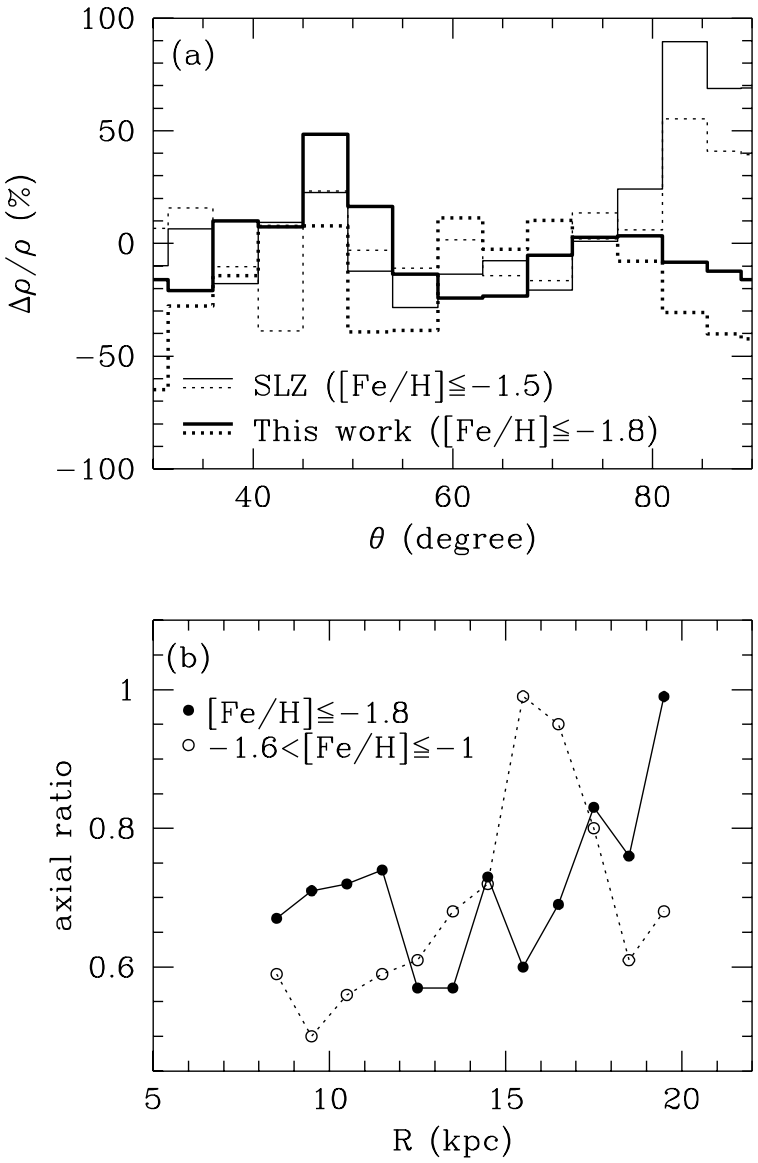

Fig. 14.— (a) Relative density deviations along elliptical fits to equidensity contours with $a = 10.5$ kpc (solid lines) and $a = 13.5$ kpc (dotted lines), when the fits are made by omitting the data points near the plane ($\theta > 80°$). The thin lines denote the SLZ sample with [Fe/H] ≤ -1.5 ($q = 0.85$ for $a = 10.5$ kpc and $q = 0.82$ for $a = 13.5$ kpc), whereas the thick lines denote our sample with [Fe/H] ≤ -1.8 ($q = 0.70$ for $a = 10.5$ kpc and $q = 0.51$ for $a = 13.5$ kpc). Note that contrary to SLZ, our sample does not show a density excess near the plane. (b) Axial ratios for the density distribution of the reconstructed halo, based on the elliptical fits to equidensity contours including stars near the plane. The filled and open circles denote our sample with [Fe/H] ≤ -1.8 and $-1.6 <$ [Fe/H] ≤ -1, respectively.

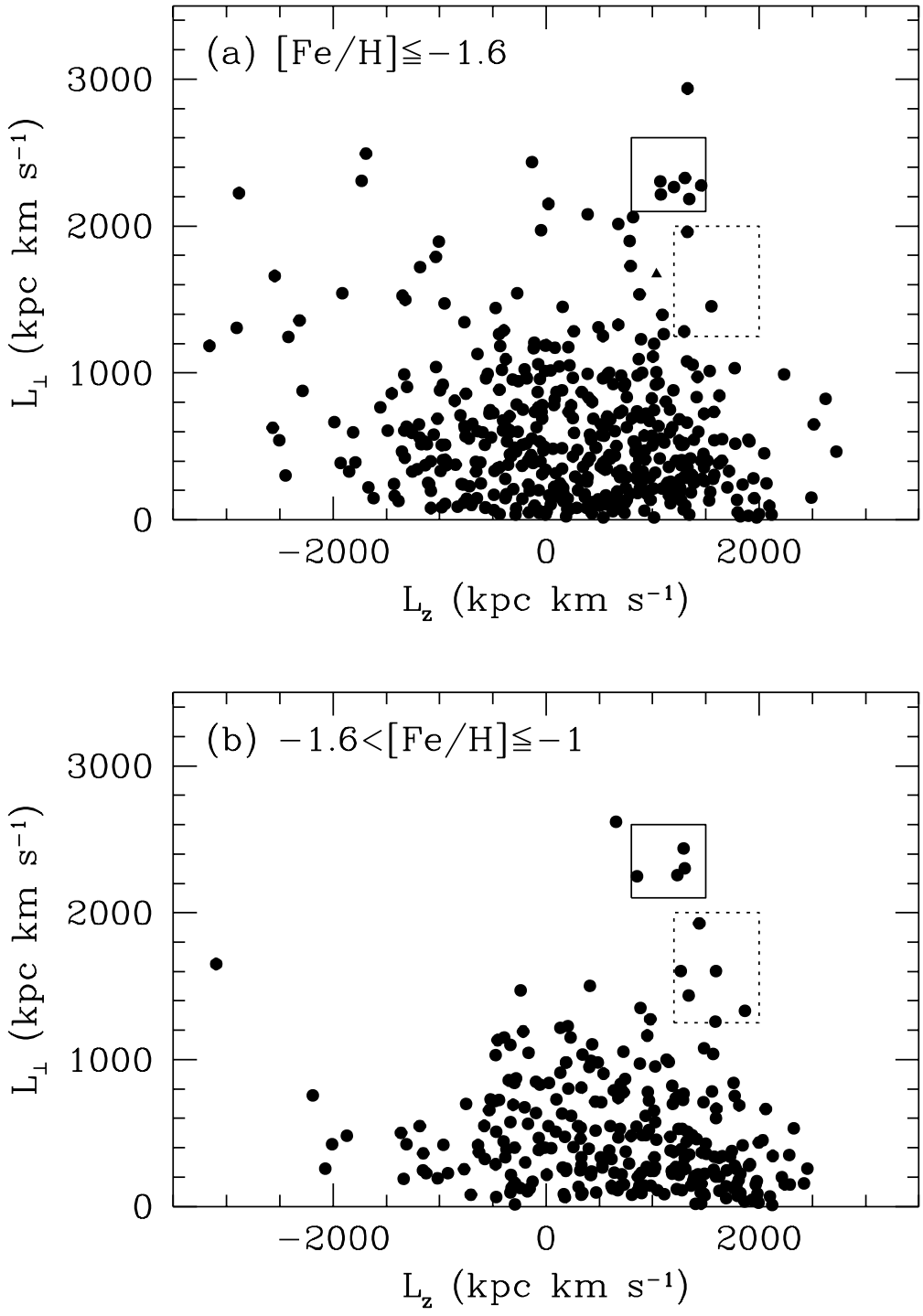

Fig. 15.— Distribution of the stars with $D < 2.5$ kpc in the angular momentum components L_z vs. $L_\perp = (L_x^2 + L_y^2)^{1/2}$, for (a) [Fe/H] ≤ -1.6 and (b) $-1.6 <$ [Fe/H] ≤ -1. The solid and dotted boxes denote the regions of the "clump" and "trail" as defined in the text. A triangle in panel (a) denotes BPS CS 22876-0040, which is assigned to a "trail" member, as discussed in the text.

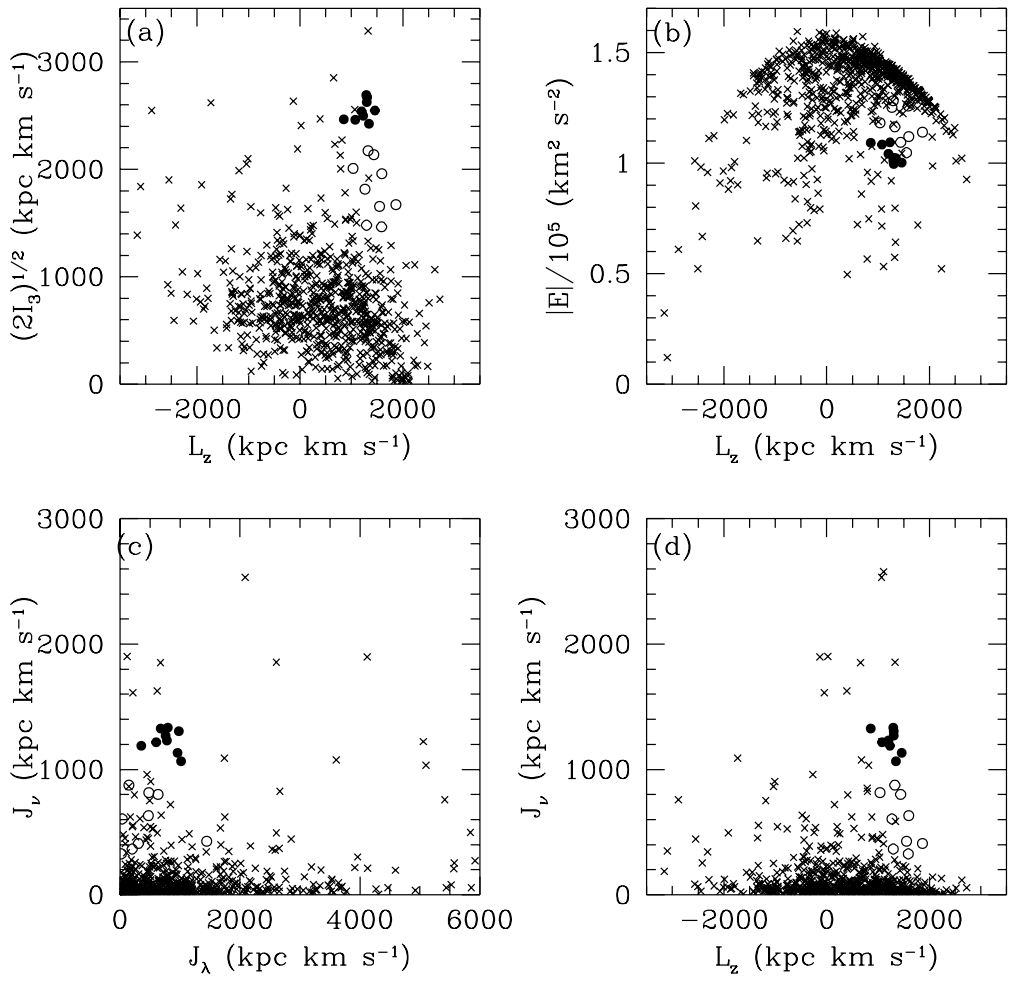

Fig. 16.— Distributions of the stars with $D < 2.5$ kpc and [Fe/H] ≤ -1, in the planes of (a) $(2I_3)^{1/2}$ vs. L_z, (b) $|E|$ vs. L_z, (c) J_ν vs. J_λ, and (d) J_ν vs. L_z. The filled and open circles denote the stars in the "clump" and "trail" regions, whereas crosses denote the rest of the stars. Note that we exclude HD 214161 from the "clump" and CS Ser from the "trail", because these stars are located at quite different regions from other member stars in the J_ν vs. J_λ diagram.

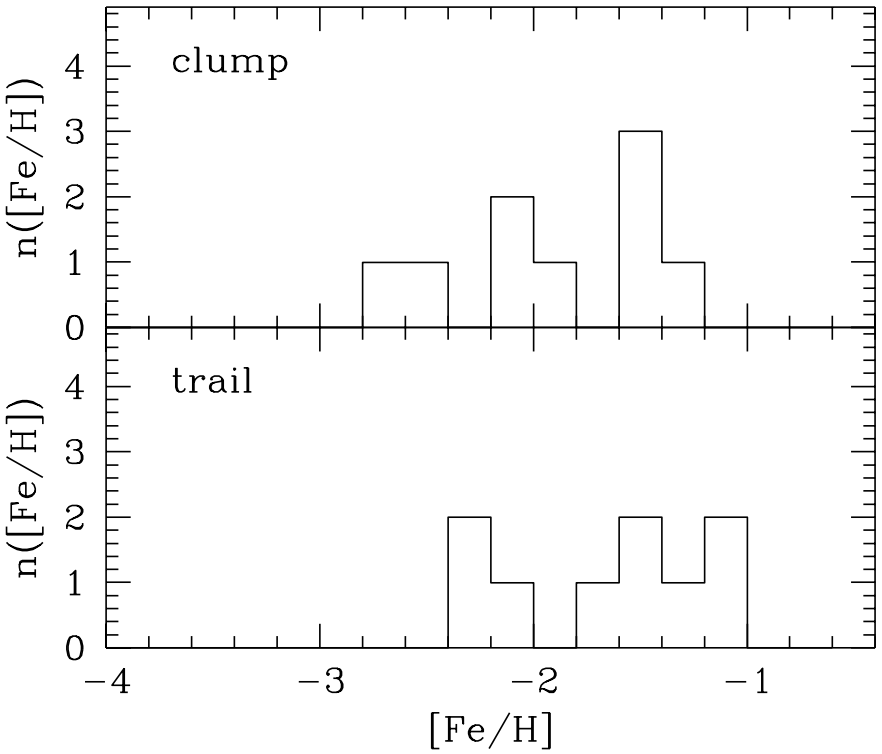

Fig. 17.— Metallicity distributions of the stars in the "clump" and "trail" regions.

This figure "fig1.gif" is available in "gif" format from:

http://arXiv.org/ps/astro-ph/0003087v1

This figure "fig6.gif" is available in "gif" format from:

http://arXiv.org/ps/astro-ph/0003087v1

This figure "fig11.gif" is available in "gif" format from:

http://arXiv.org/ps/astro-ph/0003087v1